Neurobiology of Disease 151 (2021) 105252

Contents lists available at ScienceDirect

Neurobiology of Disease

journal homepage: www.elsevier.com/locate/ynbdi

Detrimental impacts of mixed-ion radiation on nervous system function

Peter M. Klein [a,*], Vipan K. Parihar [b], Gergely G. Szabo [a], Miklós Zöldi [c], Maria C. Angulo [b], Barrett D. Allen [b], Amal N. Amin [b], Quynh-Anh Nguyen [a], István Katona [c,d], Janet E. Baulch [b], Charles L. Limoli [b], Ivan Soltesz [a,e]

[a] Department of Neurosurgery, Stanford University, Palo Alto, CA 94305, United States of America
[b] Department of Radiation Oncology, University of California, Irvine, CA 92697, United States of America
[c] Momentum Laboratory of Molecular Neurobiology, Institute of Experimental Medicine, Hungarian Academy of Sciences, 1083 Budapest, Hungary
[d] Department of Psychological and Brain Sciences, Indiana University, Bloomington, IN 47405, United States of America
[e] Department of Neurology & Neurological Sciences, Stanford University, Palo Alto, CA 94305, United States of America

ARTICLE INFO

Keywords:
Space radiation
Electrophysiology
Sharp wave-ripple
Hippocampus
Cognitive dysfunction

ABSTRACT

Galactic cosmic radiation (**GCR**), composed of highly energetic and fully ionized atomic nuclei, produces diverse deleterious effects on the body. In researching the neurological risks of GCR exposures, including during human spaceflight, various ground-based single-ion GCR irradiation paradigms induce differential disruptions of cellular activity and overall behavior. However, it remains less clear how irradiation comprising a mix of multiple ions, more accurately recapitulating the space GCR environment, impacts the central nervous system. We therefore examined how mixed-ion GCR irradiation (two similar 5-6 beam combinations of protons, helium, oxygen, silicon and iron ions) influenced neuronal connectivity, functional generation of activity within neural circuits and cognitive behavior in mice. In electrophysiological recordings we find that space-relevant doses of mixed-ion GCR preferentially alter hippocampal inhibitory neurotransmission and produce related disruptions in the local field potentials of hippocampal oscillations. Such underlying perturbation in hippocampal network activity correspond with perturbed learning, memory and anxiety behavior.

1. Introduction

Exposures to highly energetic and fully ionized atomic nuclei, such as galactic cosmic radiation (**GCR**) emitted from sources beyond our solar system, have the potential to produce a wide range of deleterious effects on the human body. Some understood risks of GCR exposure include increases in carcinogenesis and disrupted central nervous system function (Cucinotta et al. 2014; Nelson 2016). Although humans are largely screened from interactions with GCR by the magnetic field of the Earth, space radiation poses a greater threat as humans look to journey beyond the Earth to the Moon and Mars (Cucinotta et al. 2001; Cucinotta and Durante 2006; Zeitlin et al. 2013).

While the exact mechanisms through which GCR produce detrimental physiological effects remains an active area of study, at a cellular level GCR damage can arise from the production of complex, double-strand DNA breaks (Ward 1994; Asaithamby and Chen 2011) or direct disruptions of neurites (Al-Jahdari et al. 2009). GCR-induced DNA damage induces a variety of cellular effects, including decreased cell survival (Miller et al. 1998; Lee et al. 2005), altered gene expression (Ding et al. 2005; Shukitt-Hale et al. 2013), increased chromosome aberrations (Limoli et al. 2000; George et al. 2007), reduced neurogenesis (Whoolery et al. 2017) and elevated neuroinflammation (Rola et al. 2005, 2008; Parihar et al. 2018). However, at space-relevant GCR doses, the degree to which DNA damage impacts long-term nervous system functions such as cognition remains uncertain. Interestingly, even low dose exposures to protons and helium nuclei, the lightest and most abundant components of GCR that elicit relatively lower levels of complex DNA damage, are still known to produce long-lasting neurological perturbation. These effects include diminished dendritic complexity (Parihar et al. 2015a, 2015c), disrupted neurotransmission (Sokolova et al. 2015; Lee et al. 2017; Parihar et al. 2018) and deficits in behavior (Davis et al. 2015; Parihar et al. 2015a, 2018).

However, the full GCR composition also includes a range of high atomic number, high energy (**HZE**) fully ionized nuclei. While less abundant, the increasingly energetic HZE components of GCR produce higher multiplicities of ionization through triggering additional particle

* Corresponding author at: 1201 Welch Rd, Palo Alto, CA 94305, United States of America.
E-mail address: kleinp@stanford.edu (P.M. Klein).

https://doi.org/10.1016/j.nbd.2021.105252
Received 1 August 2020; Received in revised form 2 December 2020; Accepted 2 January 2021
Available online 5 January 2021

emission along their primary track and generating secondary delta ray emissions that spread laterally along sparsely ionizing tracks that significantly increase the cross section of impacted tissue (Cucinotta and Durante 2006; Autsavapromporn et al. 2013). Like proton and α-particle radiation, exposure to individual HZE ion species such as oxygen (Rabin et al. 2011; Carr et al. 2018), silicon (Rabin et al. 2011; Whoolery et al. 2017) and iron (Britten et al. 2012; Cherry et al. 2012; Haley et al. 2013) all can produce persistent behavioral and cognitive deficits.

Over the course of deep space voyages to the Moon or Mars, astronauts will be chronically exposed to elevated levels of GCR, calculated to be approximately 1.5 cGy/month (Zeitlin et al. 2013; Cucinotta et al. 2014). The high energies inherent to space radiation confound efforts to provide adequate shielding, and as a result, certain levels of exposure are inevitable (Cucinotta and Durante 2006). Typical spacecraft shielding approximately halves GCR exposures, yet integrating sufficiently substantial shielding to alleviate GCR risks would prohibitively increase spacecraft mass (Dobynde and Shprits, 2020; Simonsen et al., 2020; Slaba et al., 2016). Therefore, in the context of space travel, where astronauts need to maintain keen cognitive and decision-making skills, it is imperative to clearly understand the potential adverse impact of GCR exposure on central nervous system functionality. Furthermore, HZE ion-based radiation therapy is emerging as a potential treatment for brain, head and neck cancers, although the potential for negative impacts on nearby normal brain tissue require further investigation (Miyawaki et al. 2009; Durante et al. 2017). Fully studying the consequences of GCR irradiation on the nervous system is required to accurately assess potential risks from exposures and to accurately develop countermeasures to forestall the onset of neurocognitive decline.

As various single-ion GCR exposure paradigms have been shown to differentially disrupt cellular activity and overall behavior, it remains unclear how space-relevant doses of mixed-ion GCR may impact the central nervous system. We therefore examined how simulated, mixed-ion GCR exposure (containing combinations of protons, helium, oxygen, silicon and iron ions) influenced neuronal connectivity, functional generation of activity within neural circuits and cognitive behavior. We find that acute exposure to space-relevant doses of mixed-ion GCR preferentially alter inhibitory neurotransmission within the hippocampus and produce related disruptions in hippocampal oscillations. Such underlying perturbation in hippocampal network activity corresponds to a range of deficits in cognitive tasks.

2. Results

The goal of the current study was to determine if space-relevant doses of mixed-ion GCR induce long-lasting alterations in neurological function. We used electrophysiological and anatomical approaches to measure GCR-induced alterations in synaptic signaling among hippocampal neurons. We additionally performed *in vivo* local field potential (**LFP**) recordings to assess potential changes in hippocampal oscillations. Finally, we conducted a battery of behavioral and cognitive testing in mice to examine changes induced by mixed-ion GCR exposure (Fig. S1). Collectively, our results demonstrate that space-relevant doses of mixed-ion GCR produce persistent increases in inhibitory signaling within the CA1 region of the hippocampus, a slowing in the frequency of hippocampal sharp wave-ripples, and detriments in learning and memory. All mice were irradiated at the NASA Space Radiation Laboratory (**NSRL**) at Brookhaven National Laboratory in two batches, implementing broadly similar 5- or 6-beam mixed-ion GCR exposures (Table 1). For clarity, the specific GCR irradiation paradigm is identified for each experiment.

2.1. Mixed-ion GCR enhances inhibitory, but not excitatory, synaptic signaling with CA1

While future astronauts face a wide range of risks associated with whole-body GCR exposure, we chose to focus on the impacts of GCR irradiation on hippocampal function. There is substantial evidence that the properties of hippocampal neurons are altered by even low doses of single-ion GCR irradiation (Sokolova et al. 2015; Lee et al. 2017; Carr et al. 2018; Parihar et al. 2018).

We began by assessing whether exposure to a space-relevant dose of 30 cGy mixed-ion GCR (6-beam) produced any changes in the intrinsic electrophysiological properties of hippocampal pyramidal neurons within the CA1 superficial layer (Fig. 1). The resting membrane potential of GCR-irradiated neurons remained similar to that of control neurons (Mean difference ($\boldsymbol{M}_{\mathbf{diff}}$) = 0.97 mV, 95% CI[−1.31, 3.26]; d = −0.21, 95% CI[−0.31, 0.71]; Mixed linear modeling z-value (**MLM *z***) = 0.84, $P = 0.399$; Fig. 1A). CA1 pyramidal neurons from GCR-irradiated and control mice were also subjected to a range of brief current injections to test for changes in cell-intrinsic properties (Fig. 1B). Mixed-ion GCR exposure neither altered the input resistance of CA1 pyramidal neurons ($M_{\text{diff}} = 5.6$ MΩ, 95% CI[−8.8, 16.6]; $d = -0.22$, 95% CI [−0.34, 0.78]; MLM $z = 0.88$, $P = 0.381$; Fig. 1C), nor the amplitude of the hyperpolarization sag when neurons were injected with a − 100 pA current ($M_{\text{diff}} = 0.037$ mV, 95% CI[−0.56, 0.51]; $d = -0.03$, 95% CI [−0.51, 0.54]; MLM $z = 0.14$, $P = 0.890$; Fig. 1D). Furthermore, the excitability of CA1 pyramidal neurons was unchanged by 30 cGy of mixed-ion GCR irradiation, with the same rheobase current evoking action potentials in irradiated and control neurons ($M_{\text{diff}} = 0.037$ mV, 95% CI[−0.56, 0.51]; $d = -0.03$, 95% CI[−0.51, 0.54]; MLM $z = 0.14$, $P = 0.890$; Fig. 1B,E). Across a range of current injections, neurons from both groups displayed equivalent action potential firing frequencies ($F(1,549) = 0.009$, $P = 0.926$, two-way ANOVA, Fig. 1F) and exhibited similar action potential firing thresholds ($M_{\text{diff}} = 1.89$ mV, 95% CI [−0.30, 4.13]; $d = 0.43$, 95% CI[−0.10, 0.91]; MLM $z = 1.06$, $P = 0.290$; Fig. 1G). Altogether, we find no evidence that mixed-ion GCR irradiation alters the intrinsic properties of CA1 pyramidal neurons.

While 30 cGy mixed-ion GCR exposure does not change the intrinsic properties of CA1 pyramidal neurons, low doses of single-ions are known to disrupt dendritic spines and reduce markers of excitatory synapses within the hippocampus (Parihar et al. 2015c; Carr et al. 2018). Thus, we next examined whether excitatory synapses within CA1 are perturbed by 30 cGy GCR irradiation (5-beam). Excitatory presynaptic terminals in CA1 stratum radiatum of male mice were immunohistochemically (**IHC**) labeled for vesicular glutamate transporter 1 (**VGluT1**), combined with Bassoon staining to support localization within axonal terminals, prior to confocal imaging (Fig. 2A**)**. Examining areas of colocalization between VGluT1 and Bassoon, we did not observe

Table 1
Ion compositions of the utilized simulated GCR paradigms.

5-beam Mixed-ion GCR				6-beam Mixed-ion GCR				
Ion	Energy (MeV/n)	Relative Dose (%)	30 cGy Dose (cGy)	Ion	Energy (MeV/n)	Relative Dose (%)	5 cGy Dose (cGy)	30 cGy Dose (cGy)
^{1}H	1000	30	9.0	^{1}H	1000	35	1.75	10.5
^{16}O	400	10	3.0	^{28}Si	600	1	0.05	0.3
^{4}He	400	20	6.0	^{4}He	250	18	0.9	5.4
^{28}Si	600	10	3.0	^{16}O	350	6	0.3	1.8
^{1}H	1000	30	9.0	^{56}Fe	600	1	0.05	0.3
				^{1}H	250	39	1.95	11.7

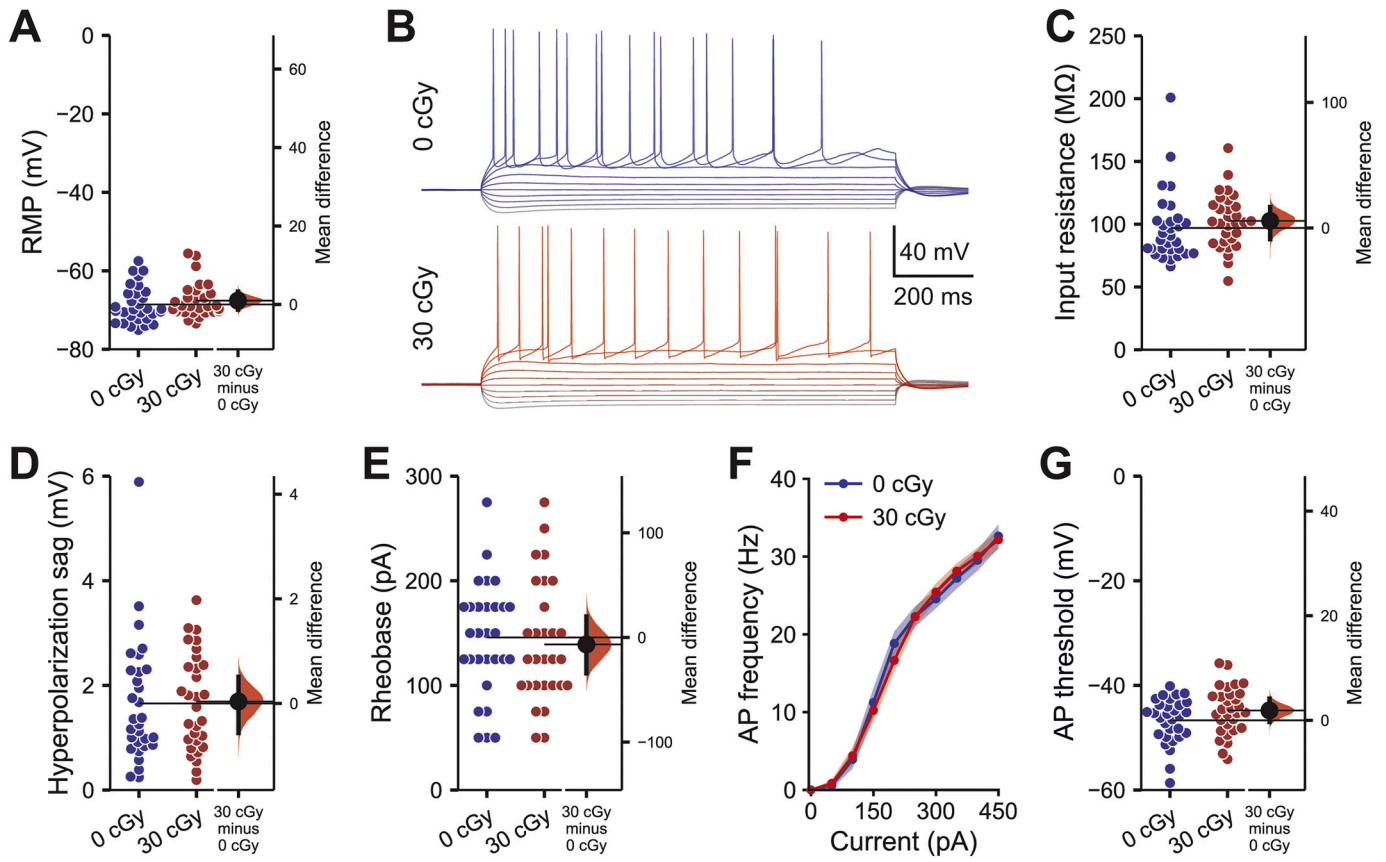

Fig. 1. Low-dose, mixed-ion, GCR irradiation does not alter the intrinsic electrophysiological properties of CA1 pyramidal neurons. All data are from whole cell current clamp recordings of CA1 pyramidal neurons from the superficial layer of the dorsal hippocampus, 4 months after exposure to 30 cGy GCR (6-beam). A, Resting membrane potential (RMP) was unchanged between groups. B, Representative examples of responses to a range of brief current injections in 0 cGy and 30 cGy neurons. There was no alteration in the input resistance (C), sag during a − 100 pA hyperpolarizing current injection (D), or rheobase current required to evoke an action potential (E) between the treatment groups. F, Action potential (AP) frequency remained equivalent across a range of current injections and the threshold potential for action potential initiation remained unchanged (G). $N = 30$ cells/6 animals for both the 0 cGy and 30 cGy grouped data. Gardner-Altman estimation plots show raw data on the left axis and a bootstrapped sampling distribution on the right axis. A black dot depicts the mean difference between groups and the 95% confidence interval is indicated by the ends of the vertical black bars. Data are presented as Mean ± SEM for *F*. *$P < 0.05$ (mixed linear model regression or two-way ANOVA).

a change in the number of doubly labeled terminals following low-dose, mixed-ion, GCR irradiation ($M_{diff} = 35.8$, 95% CI[−11.8, 97.7]; $d = 0.46$, 95% CI[−0.24, 1.14]; MLM $z = 0.84$, $P = 0.401$; Fig. 2B). Furthermore, the normalized intensity of VGluT1 staining, whether overall (MLM $z = 0.31$, $P = 0.760$; data not shown), or specifically within colocalized objects was similarly unchanged in irradiated mice ($M_{diff} = −0.07\%$, 95% CI[−0.78, 0.77]; $d = −0.06$, 95% CI[−0.74, 0.73]; MLM $z = 0.10$, $P = 0.920$; Fig. 2C). Therefore, the number and size of excitatory synapses within the CA1 stratum radiatum appear to be largely unchanged by low-dose, mixed-ion, GCR irradiation. However, more subtle shifts in the association between VGluT1-positive presynaptic vesicle zone and the Bassoon-positive active zone could occur in response to alterations in excitatory signaling (Glebov et al. 2016). A wide range of additional protein interactions are required for normal synaptic signalling, with several elements showing alterations in other GCR irradiation paradigms, including postsynaptic density protein 95 (**PSD-95**), drebrin 1, synapsin 1, and synaptophysin (Kiffer et al., 2018; Parihar et al., 2016). Thus, we next sought to directly measure the synaptic inputs received by CA1 pyramidal neurons.

To independently assess whether GCR irradiation (6-beam) alters hippocampal connectivity, we separately performed electrophysiological recordings of the spontaneous excitatory and inhibitory postsynaptic activity received by CA1 pyramidal neurons (Fig. 3). We have previously observed that low-dose, single-ion irradiation is sufficient to disrupt hippocampal synaptic signaling (Sokolova et al. 2015; Lee et al. 2017). However, CA1 pyramidal neuron spontaneous excitatory postsynaptic current (**sEPSC**) frequency following mixed-ion GCR irradiation matches that of control animals ($M_{diff} = −0.35$ Hz, 95% CI[−1.08, 0.29]; $d = −0.35$, 95% CI[−1.03, 0.39]; MLM $z = 1.11$, $P = 0.267$; Fig. 3A-B). To test for differences in the sEPSC properties of individual neurons, all sEPSCs detected within a 200 *s* recording period from each cell were averaged together to generate a standard profile (Fig. 3C). Here too, simulated GCR irradiationdid not alter average sEPSC amplitude ($M_{diff} = 0.08$ pA, 95% CI[−1.59, 1.90]; $d = 0.03$, 95% CI[−0.69, 0.80]; MLM $z = 0.09$, $P = 0.930$; Fig. 3D), charge transfer ($M_{diff} = −2.34$ pC, 95% CI[−17.8, 14.0]; $d = −0.10$, 95% CI[−0.84, 0.63]; MLM $z = 0.27$, $P = 0.786$; Fig. 3E) or rise time ($M_{diff} = −0.013$ ms, 95% CI[−0.32, 0.24]; $d = −0.03$, 95% CI[−0.78, 0.76]; MLM $z = 0.05$, $P = 0.962$; Fig. 3F). Matched experiments in mice subjected to the 5-beam composition of GCR irradiation (**Fig. S2** and **Table S1-2**) similarly demonstrate a minimal impact of low-dose GCR exposure on both the intrinsic properties and sEPSC activity of CA1 neurons. Thus, both IHC labeling and electrophysiological recordings consistently demonstrate that excitatory synaptic signaling to CA1 pyramidal neurons is not substantially altered by low-dose, mixed-ion, GCR irradiation.

While we do not observe an impact of mixed-ion GCR irradiation on excitatory synaptic signaling to CA1 pyramidal neurons, we have previously observed that low-dose proton irradiation selectively upregulates inhibitory signaling by subpopulations of hippocampal interneurons (Lee et al. 2017). Therefore, we proceeded to evaluate

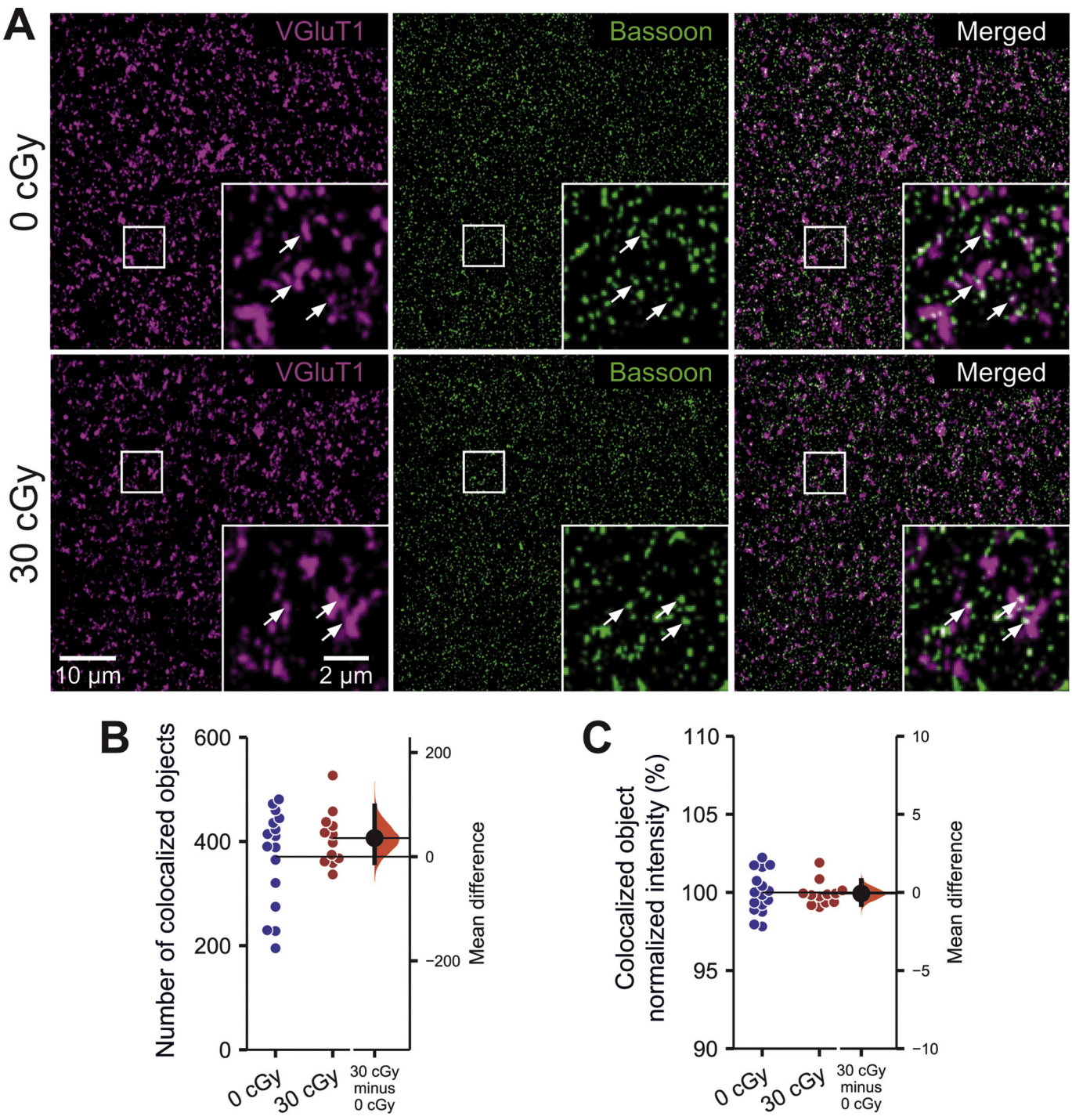

Fig. 2. Excitatory presynaptic terminals in CA1 are not altered by mixed-ion GCR irradiation. Coronal brain sections containing the dorsal hippocampus were prepared 3 months after exposure to 30 cGy mixed-ion GCR (5-beam). A, Immunofluorescence colocalization between VGluT1 (magenta) and Bassoon (green) identified putative excitatory presynaptic terminals within CA1 stratum radiatum of GCR irradiated and control mice. Insets show an enlarged region of each image, with arrows indicating examples of overlapping VGluT1 and Bassoon. GCR irradiation did not alter the number (B) or intensity (C) of VGuT1 and Bassoon colabeled presynaptic terminals. N = 4/3 animals, 16/12 sections (0 cGy and 30 cGy, respectively). Gardner-Altman estimation plots show raw data on the left axis and a bootstrapped sampling distribution on the right axis. A black dot depicts the mean difference between groups and the 95% confidence interval is indicated by the ends of the vertical black bars.

whether low-dose, mixed-ion, GCR irradiation (6-beam) alters inhibitory postsynaptic signaling received by CA1 pyramidal neurons (Fig. 3G-L). Following mixed-ion irradiation, the frequency of spontaneous inhibitory postsynaptic currents (**sIPSC**) remains similar to that of control mice (M_{diff} = 0.01 Hz, 95% CI[−0.40, 0.44]; d = 0.02, 95% CI [−0.76, 0.94]; MLM z = 0.06, P = 0.951; Fig. 3H). However, when comparing sIPSC properties (Fig. 3I), we observe a large effect-size elevation in the sIPSC amplitude of GCR irradiated mice relative to control animals (M_{diff} = 5.54 pA, 95% CI[1.04, 10.09]; d = 0.95, 95% CI [0.08, 1.80]; MLM z = 2.01, P = 0.044; Fig. 3J). The increase in sIPSC amplitude is not accompanied by a change in the charge transfer of inhibitory currents (M_{diff} = 44.9 pC, 95% CI[−2.1, 105.5]; d = 0.63,

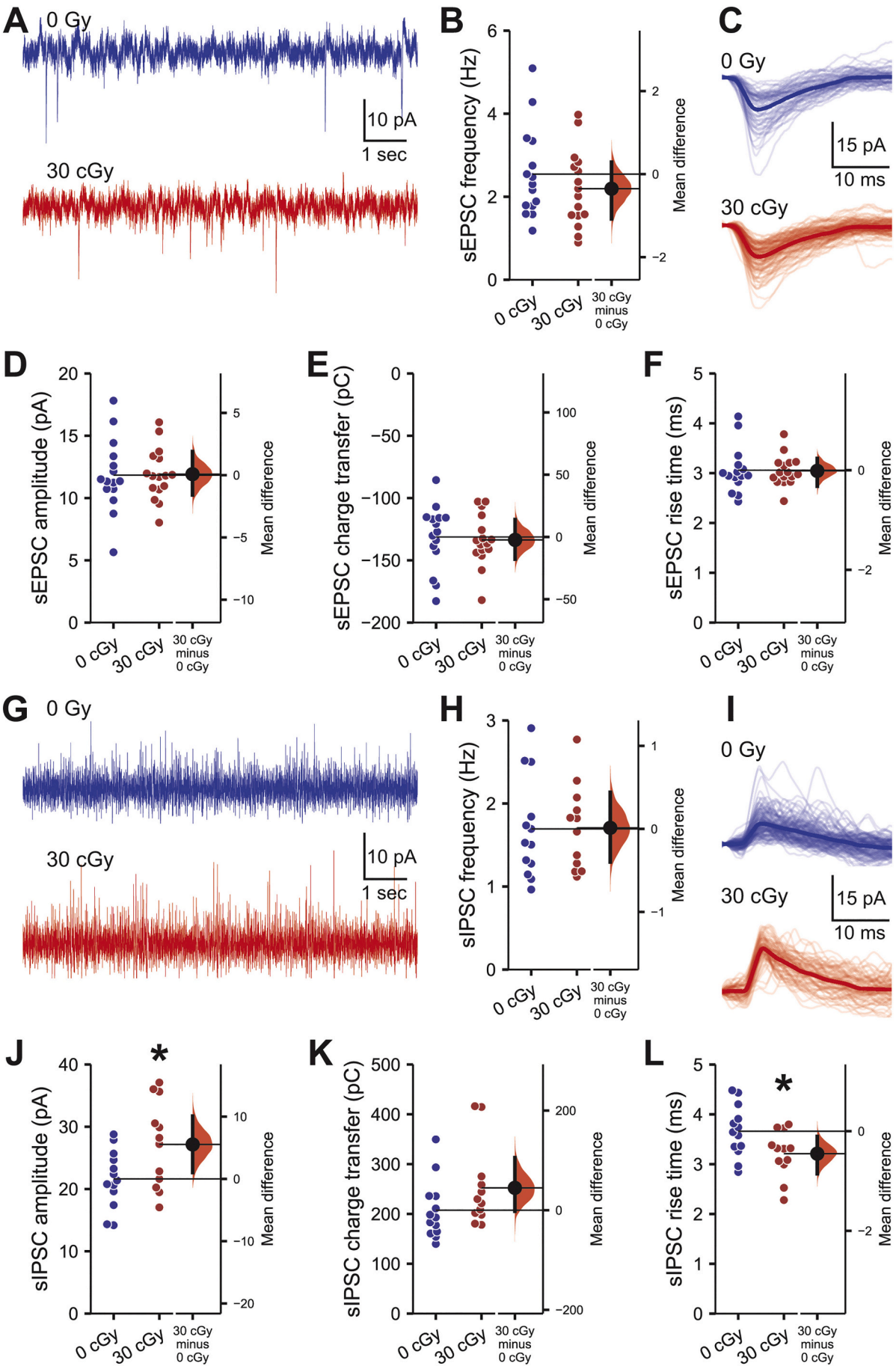

(caption on next page)

Fig. 3. Mixed-ion GCR irradiation preferentially enhances inhibitory synaptic signaling. All data are from whole cell voltage clamp recordings of CA1 pyramidal neurons from the superficial layer of the dorsal hippocampus, 4 months after exposure to 30 cGy GCR (6-beam). A, Representative examples of spontaneous excitatory postsynaptic currents (sEPSCs) recordings from 0 cGy and 30 cGy neurons. B, The frequency of sEPSCs was equivalent between 0 Gy and 30 cGy neurons. C, Aligned examples of sEPSCs in representative 0 Gy and 30 cGy neurons. Light lines show individual sEPSCs, while the darker line displays the average sEPSC during a 200 s recording from that neuron. sEPSC amplitude (D), charge transfer (E) and rise time (F) were all similar between groups. G, Representative examples of spontaneous inhibitory postsynaptic current (sIPSC) recordings from 0 cGy and 30 cGy neurons. While the frequency of sIPSCs was equivalent between 0 Gy and 30 cGy neurons (H), sIPSC amplitude increased after irradiation (—I–J). K, sIPSC charge transfer remained similar between groups. L, sIPSC rise time decreased following irradiation. N = 3/3 animals, 15/16 cells for sEPSCs and N = 3/3 animals, 13/12 cells for sIPSCs (0 cGy and 30 cGy, respectively). Gardner-Altman estimation plots show raw data on the left axis and a bootstrapped sampling distribution on the right axis. A black dot depicts the mean difference between groups and the 95% confidence interval is indicated by the ends of the vertical black bars. *$P < 0.05$ (mixed linear model regression).

95% CI[−0.19, 1.34]; MLM $z = 1.53$, $P = 0.126$; Fig. 3K). We also observed a large effect-size decrease in the sIPSC rise times of GCR irradiated animals ($M_{diff} = -0.45$ ms, 95% CI[−0.85, −0.10]; $d = -0.92$, 95% CI[−1.68, −0.09]; MLM $z = 2.23$, $P = 0.021$; Fig. 3L).

Coordinated synaptic signaling among hippocampal neurons underlie a variety of network-level patterns of oscillatory activity (Buzsáki 2002, 2015). Perturbations of either excitatory (Korotkova et al. 2010) or inhibitory (Ponomarenko et al. 2004; Koniaris et al. 2011) signaling within the hippocampus is sufficient to alter rhythmic activity and disrupt animal behavior. Thus, we next examined whether mixed-ion GCR irradiation produces any alterations in hippocampal oscillations.

2.2. Hippocampal oscillations are altered by mixed-ion GCR exposure

Oscillatory activity within the hippocampus varies as animals shift among behavioral states, such as between active exploration *versus* quiet wakefulness (Vanderwolf 1969). As mice move around an environment, the membrane potentials of large ensembles of CA1 pyramidal neurons synchronously oscillate at theta frequencies (4–10 Hz) in response to a mixture of inputs, including cholinergic and GABAergic inputs from the medial septum (Green and Arduini 1954; Buzsáki et al. 1983), excitatory signaling from the entorhinal cortex (Brankačk et al. 1993) and inhibitory signaling from local interneurons (Varga et al. 2014). Such synchronous membrane potential oscillations appear as the theta rhythm during hippocampal LFP recordings. Conversely, mice at rest display periodic sharp wave-ripples (90–200 Hz), observable in hippocampal LFP recordings, induced by excitatory inputs from CA3 to CA1 pyramidal neurons that then recruit recurrent signaling from local inhibitory interneurons (Soltesz and Deschênes 1993; Ylinen et al. 1995; Buzsáki 2015). Due to our observation that mixed-ion GCR irradiation augments the amplitude of inhibitory signaling onto CA1 pyramidal neurons, we next recorded the hippocampal LFP of mice on a spherical treadmill (Fig. 4). We then analyzed the hippocampal rhythms present in the LFP recordings while mice exhibited running or resting behavior (Fig. 4A-B).

Mixed-ion GCR irradiation (5-beam) did not alter the amplitude (root mean square) of running-associated hippocampal oscillations in the theta frequency range ($t = 0.59$, $P = 0.577$, *t*-test). Likewise, we observe no alteration in the delta (0.5–4 Hz; $t = 2.14$, $P = 0.076$, *t*-test), low gamma (20–55 Hz; $t = 0.32$, $P = 0.760$, *t*-test), gamma (20–95 Hz; $t = 0.64$, $P = 0.546$, *t*-test) or high gamma (85–135 Hz; $t = 0.41$, $P = 0.698$, *t*-test) frequency ranges during running (Fig. 4C). Furthermore, mixed-ion irradiation neither changes the power ($t = 0.10$, $P = 0.921$, *t*-test; Fig. 4D), nor the frequency ($t = 0.29$, $P = 0.783$, *t*-test; Fig. 4E) of rest-associated sharp wave-ripple oscillations. The bilateral co-occurrence of ripples also remains equivalent following mixed-ion GCR irradiation to that of control animals ($t = 1.38$, $P = 0.217$, *t*-test; Fig. 4F). However, we do observe that the average frequency of the underlying oscillations within ripples becomes slower after low-dose GCR irradiation than in control mice ($t = 4.34$, $P = 0.005$, *t*-test; Fig. 4G), which is also observed as an increased likelihood of lower frequency ripples in a kernel density estimate of all detected events (Fig. 4H).

Such a decrease in intra-ripple frequency is consistent with an enhancement of hippocampal GABAergic signaling, as also occurs following acute pharmacological manipulations (Ponomarenko et al. 2004; Koniaris et al. 2011). Similarly, pharmacological augmentation of hippocampal GABAergic signaling is sufficient to diminish LTP and performance in memory tasks (Cheng et al. 2006; Martin et al. 2009). Therefore, we next examined whether acute exposures to low doses of mixed-ion GCR is sufficient to induce adverse behavioral deficits.

2.3. Mixed-ion GCR exposure induces cognitive behavioral deficits

As complex animal behavior depends upon properly tuned neuronal interactions at cellular and network levels, we next investigated whether the increased amplitude of hippocampal inhibitory signaling and decreased frequency of memory-associated sharp wave-ripples were likewise associated with cognitive deficits following mixed-ion GCR irradiation. Similar to our previous studies that linked single-ion exposures to detrimental behavioral alterations (Parihar et al. 2015a, 2018), we applied a battery of behavior tests to examine how 5-beam, mixed-ion, GCR irradiation might impair core cognitive properties that could present a risk to astronauts during future deep space exploration.

Recognition memory assays, such as the novel object recognition (**NOR**) task, rely upon proper signaling among the hippocampus and medial prefrontal cortex (Finlay et al. 2015; Ko 2017). We did not observe any difference from control in the total time mice interacted with objects during the NOR training phase ($F(2,33) = 0.18$, $P = 0.838$, one-way ANOVA; Fig. 5A) resulting from either 5 cGy ($M_{diff} = 4.4$ s, 95% CI[−10.3, 20.7]; $d = 0.22$, 95% CI[−0.62, 1.03]) or 30 cGy mixed-ion GCR irradiation ($M_{diff} = -0.9$ s, 95% CI[−17.5, 19.3]; $d = -0.04$, 95% CI[−0.99, 0.79]). Thus, there appear to be no confounding alterations in general locomotion or exploratory behavior. However, GCR irradiation did alter the ability of mice to differentiate a novel object ($F(2,33) = 8.42$, $P = 0.0011$, one-way ANOVA; Fig. 5B), with 30 cGy animals displaying a large effect-size decrease in discrimination ability relative to control mice ($M_{diff} = -35.9$, 95% CI[−51.3, −17.3]; $d = -1.66$, 95% CI[−2.92, −0.43], $P < 0.001$). While not significantly altered relative to control mice, 5 cGy irradiation did produce a medium effect-size decrease in novel object discrimination ($M_{diff} = -13.1$, 95% CI[−28.2, 3.3]; $d = -0.64$, 95% CI[−1.55, 0.27], $P = 0.316$), although this was smaller than that produced by 30 cGy ($P = 0.038$). Such diminished NOR performance suggest that normal recognition memory can be disrupted by exposure to even low doses of mixed-ion GCR radiation. Appropriate object discrimination in such tasks requires proper connectivity and processing within the hippocampus, medial prefrontal cortex and perirhinal cortex (Squire et al. 2004; Warburton and Brown 2015), suggesting that the deficits induced by GCR irradiation may extend to multiple brain regions.

To extend our assessments to other forms of memory, we also evaluated whether mixed-ion GCR irradiation (5-beam) perturbs spatial learning and memory functions using the Morris water maze test (D'Hooge and De Deyn, 2001). GCR irradiation did not alter the capacity of mice to learn the location of a submerged platform, relative to control animals, across 7 days of training sessions ($F(2,218) = 0.103$, $P = 0.902$, two-way ANOVA, Fig. 5C), including when the platform was relocated to a different quadrant after the 4th day of training. Subsequently, in a probe trial with the platform removed we observed differences in the amount of time the different treatment groups spent searching in the target quadrant that previously held the platform (Fig. 5D). Control mice

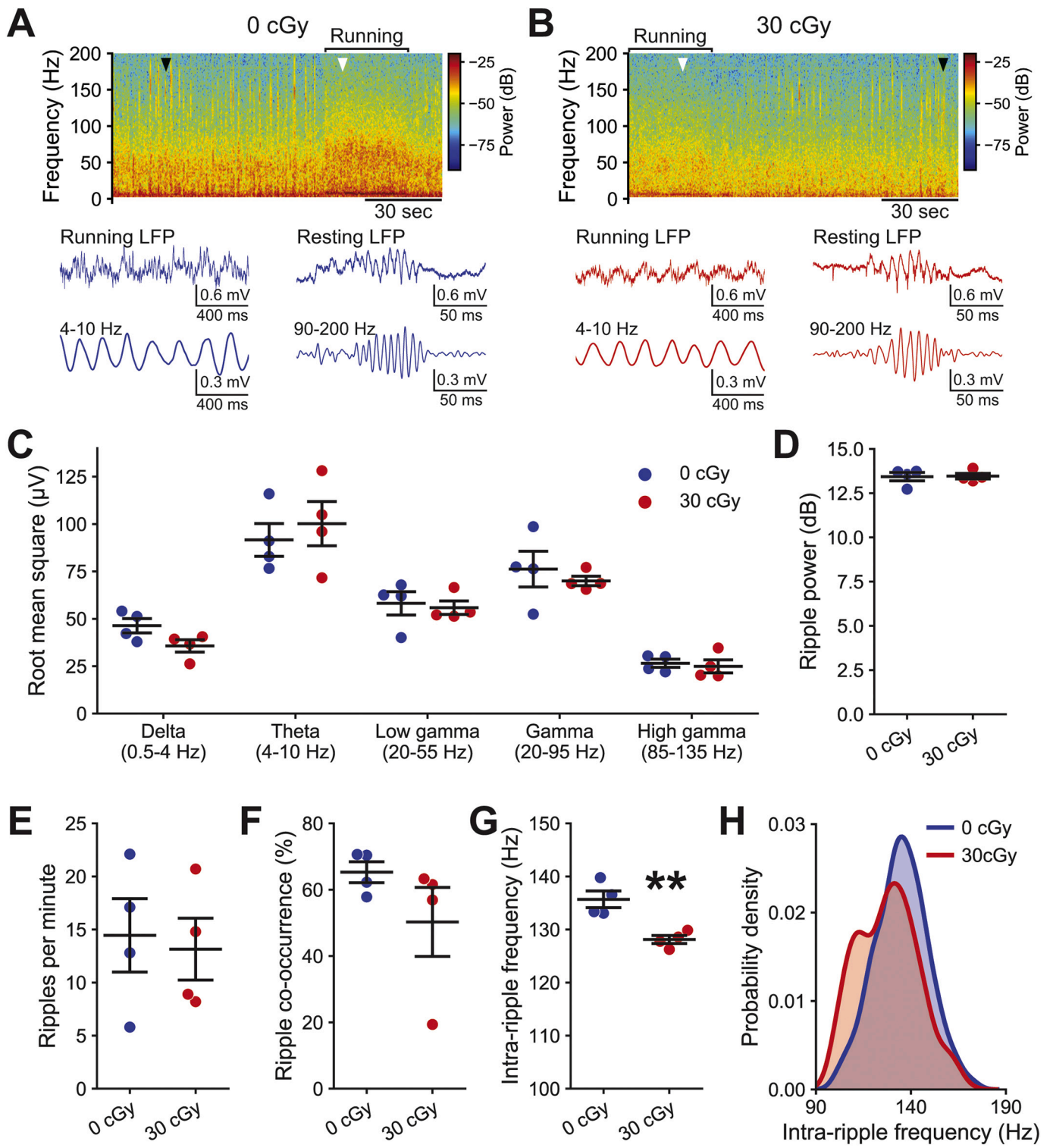

Fig. 4. Memory-associated hippocampal oscillations are disrupted by mixed-ion GCR irradiation. At 2 months after exposure to 30 cGy GCR (5-beam), local field potential (LFP) was recorded from CA1 stratum pyramidale. Representative examples of the frequency spectra of hippocampal LFP from a control (A) and GCR irradiated (B) mouse during periods of running or resting (top). Examples of raw and theta-filtered running-associated LFP (bottom left, white arrowhead). Examples of raw and ripple-filtered rest-associated LFP (bottom right, black arrowhead). C, Mixed-ion GCR irradiation did not alter running-associated rhythms. Neither the power in the 90–200 Hz ripple band of the resting LFP (D), nor the frequency of ripple occurrence (E) was altered following GCR irradiation. F, The co-occurrence of bilateral ripples was similar in GCR irradiated and control mice. Mixed-ion GCR irradiation slows the intra-ripple oscillatory frequency within animals (G) and also appears to increase the likelihood of slower ripples in a kernel density estimate of all detected events (H). N = 4/4 animals (0 cGy and 30 cGy, respectively) for all plots showing grouped data. Data are presented as Mean ± SEM for *C-G*. $^{**}P < 0.01$ (*t*-test).

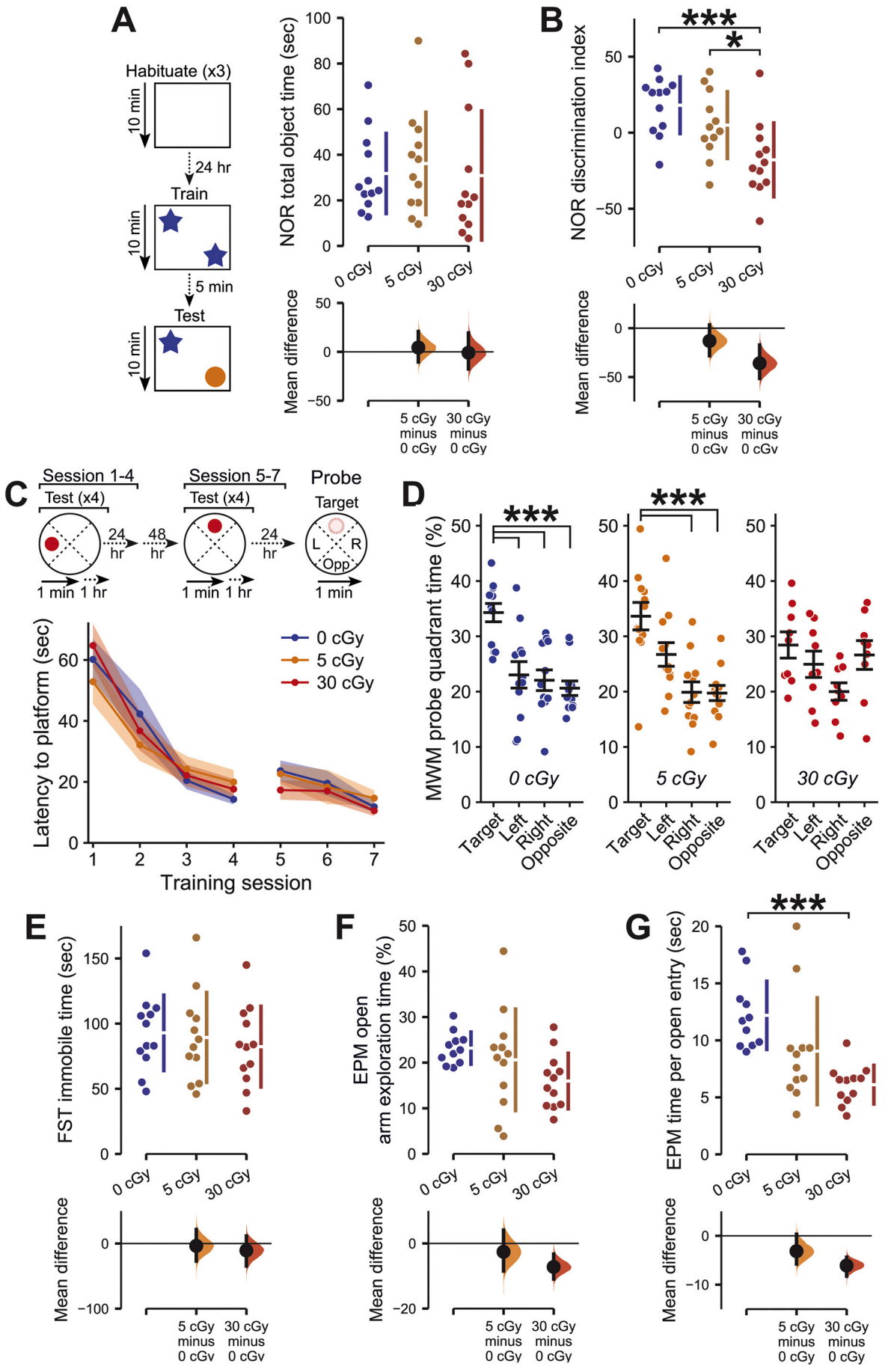

(caption on next page)

Fig. 5. Mixed-ion GCR irradiation disrupts cognition and elicits anxiety-like behavior. Behavioral testing was conducted 6–10 weeks following exposure to 5 or 30 cGy GCR (5-beam). While overall exploration was similar during the novel object recognition (NOR) task (A), irradiation disrupted the ability of mice to differentiate novel objects (B). C, Morris water maze (MWM) testing assessed mouse spatial learning of a platform location, including a platform relocation and probe task (top). GCR irradiation did not alter acquisition of platform location (bottom). D, During the probe trial of the MWM, 0 cGy (left) and 5 cGy (middle) animals mostly searched in the target quadrant that previously contained the platform, whereas 30 cGy mice searched equivalently throughout the maze (right). E, GCR irradiation did not alter depression-like behavior in the forced swim test (FST). Mice exposed to 30 cGy did not spend significantly less time in the open arms during the elevated plus maze (EPM) task (F), but showed anxiety-like behavior by avoiding long entries into the open arms (G). $N = 12/12/12$ animals in *A-B, E-G*, $N = 12/12/12$ animals in *C* and $N = 12/12/9$ in *D* (0 cGy, 5 cGy and 30 cGy, respectively). Cumming estimation plots show raw data on the top axis including SD shown with vertical bars and a bootstrapped sampling distribution on the bottom axis. A black dot depicts the mean difference between groups and the 95% confidence interval is indicated by the ends of the vertical black bars. Some data are presented as Mean ± SEM in *C-D*. $^{*}P < 0.05$ and $^{***}P < 0.001$ (two-way ANOVA).

displayed a clear quadrant preference during the probe trial ($F(3,44) = 11.51$, $P < 0.001$, one-way ANOVA), searching more in the target quadrant that formerly held the platform than in any of the other quadrants (Left: $P < 0.001$; Right: $P < 0.001$; Opposite: $P < 0.001$). Mice that received 5 cGy GCR irradiation still displayed strong quadrant preference ($F(3,44) = 10.87$, $P < 0.001$, one-way ANOVA), dwelling in the target quadrant more than some (Right: $P < 0.001$; Opposite: $P < 0.001$), but not all other quadrants (Left: $P < 0.085$). However, 30 cGy mice did not display a quadrant preference in the probe trial ($F(3,32) = 2.56$, $P = 0.072$, one-way ANOVA). Spatial reference memory deficits as we observed in the probe trial can arise from hippocampal, striatal, or insular cortex disruptions (Bermudez-Rattoni et al. 1991; Riedel et al. 1999; Setlow and McGaugh 1999).

Finally, we investigated whether mixed-ion GCR irradiation (5-beam) altered the internalizing behavior of animals, such as the persistent increases in anxiety- and depression-like behavior we observe in mice following exposures to single-ion radiation (Parihar et al. 2016, 2018). During forced swim testing, we did not observe any depression-like increases in immobility ($F(2,33) = 0.35$, $P = 0.706$, one-way ANOVA; Fig. 5E), whether in mice exposed to 5 cGy ($M_{diff} = -3.5$ s, 95% CI[−26.8, 21.5]; $d = -0.11$, 95% CI[−0.95, 0.72]) or 30 cGy ($M_{diff} = -10.6$ s, 95% CI[−34.4, 11.6]; $d = -0.35$, 95% CI[−1.21, 0.50]) GCR irradiation. In an elevated plus maze test of anxiety-like behavior, there was no overall impact of GCR irradiation on the time mice spent in the more exposed open arms ($F(2,32) = 2.63$, $P = 0.088$, one-way ANOVA; Fig. 5F) or the number of open arm entries ($F(2,32) = 2.88$, $P = 0.071$, one-way ANOVA; data not shown), although there was a large-effect size decrease in the open arm exploration time of 30 cGy animals ($M_{diff} = -7.21\%$, 95% CI[−10.92, −3.26]; $d = -1.44$, 95% CI[−2.47, −0.35]). However, mixed-ion GCR irradiation did alter how long animals remained in the open arms during individual entries ($F(2,32) = 9.38$, $P < 0.001$, one-way ANOVA; Fig. 5G). There was a large effect-size decrease in the time per open arm entry of 30 cGy mice ($M_{diff} = -6.08$ s, 95% CI[−8.24, −4.38]; $d = -2.53$, 95% CI[−3.31, −1.71], $P < 0.001$), whereas the reduction in 5 cGy animals was not significant ($M_{diff} = -3.14$ s, 95% CI[−5.77, 0.31]; $d = -0.79$, 95% CI[−1.98, 0.27], $P = 0.080$). Thus, higher doses of mixed-ion GCR irradiation appeared to increase the anxiety-like behavior of mice.

3. Discussion

As NASA and other organizations continue to advance plans to return humans to the Moon and beyond, it is becoming increasingly important to understand the potential health consequences astronauts will face from prolonged exposures to ionizing radiation. Past studies have well established that acute exposures to GCR radiation at the doses astronauts would experience over the course of a mission to Mars produce persistent neurological deficits (Rabin et al. 2011; Britten et al. 2012; Cherry et al. 2012; Haley et al. 2013; Lee et al. 2017; Parihar et al. 2018). However, the vast majority of previous studies have only evaluated the isolated impact of acute exposures to single ions, rather than a sequential multi-ion mixture that more closely recapitulates the actual variety of GCR particle types that astronauts will face (Nelson 2016). Different GCR ions possess distinct microdosimetric properties that distinguish and define the type, and relative amounts of cellular damage induced. Thus, whether such multi-beam exposures might lead to additive, synergistic or some combination of effects also remains uncertain (Norbury et al. 2016; Huang et al. 2020). Although the 5- and 6-beam simulations of GCR exposures that we evaluated do not recapitulate the precise spectral characteristics that astronauts will experience in space (Simonsen et al. 2020), our study still provides critically needed insight into how exposure to a diverse field of energetic particles alters nervous system function across a range of functional levels.

While our 5- and 6-beam, mixed-ion, simulations of GCR exposures were substantially similar, we acknowledge that the specific importance of minor differences in GCR composition on how the nervous system becomes disrupted remains unresolved. The electrophysiological measurements we replicated in mice from both mixed-ion paradigms displayed generally consistent results, indicating that 5- and 6-beam GCR irradiation similarly impacted pyramidal neuron intrinsic properties and excitatory synaptic inputs. The one difference we do observe is that only 5-beam GCR irradiation reduced neuronal action potential firing frequencies. Few previous studies have directly examined changes in hippocampal neuronal excitability following GCR irradiation, with 50 cGy proton (Sokolova et al., 2015) and 18 cGy chronic neutron irradiation (Acharya et al., 2019) decreasing pyramidal neuronal excitability, while 50 cGy proton irradiation had no impact on interneuron intrinsic properties (Lee et al., 2017). Understanding the particular contributions of individual irradiation parameters to disrupting neuronal properties will require further investigation. Nevertheless, due to their many similarities, we jointly consider the mechanisms and consequences of mixed-ion exposures to 5- and 6-beam GCR irradiation throughout the remainder of our discussion. Regardless of any small differences between our 5- and 6-beam GCR paradigms, our investigation is the first to provide important insights into how nervous system function at a neuronal, network and behavioral scale is altered by GCR irradiation involving complex mixtures of several distinct ions.

Given the morphological changes such as decreases in dendritic complexity and spine density that occur following models of single- (Parihar et al. 2015c, 2016; Carr et al. 2018) or dual-ion irradiation (Kiffer et al., 2018, 2020), we had anticipated that mixed-ion GCR irradiation could alter the intrinsic properties of hippocampal neurons. One potential reason for the lack of changes in hippocampal neuron intrinsic electrical properties after mixed-ion irradiation could be the differential impacts of various constituent ions at the delivered doses. For example, neuronal input resistance is reduced by exposure to 100 cGy of protons (Sokolova et al. 2015), but remains unchanged by 50 cGy protons (Lee et al. 2017) and increases after 5 cGy ^{4}He irradiation (Parihar et al. 2018). Homeostatic plasticity mechanisms may also enable neurons to produce compensatory shifts in membrane channel conductances that are sufficient to stabilize other intrinsic properties in response to low-dose GCR exposures (Sokolova et al. 2015). However, the extent to which such adaptive responses may mask underlying neuronal network disruptions and limit the capacity of neurons to properly respond to additional insults will require further study.

Examining the impact of mixed-ion GCR irradiation on signaling among neurons indicated differential effects on distinct elements of the hippocampal network. Our anatomical experiments suggest that mixed-ion GCR irradiation may slightly increase formation of excitatory synapses within the hippocampus. Such changes could correspond with the

increased AMPA receptor subunit GluR1 phosphorylation that occurs after 50 cGy proton irradiation, thus promoting receptor trafficking into the synapse (Parihar et al. 2015a). NMDA receptor subunit GluN2B transcription is also upregulated by 10 cGy ^{16}O irradiation, although GluN1 subunits conversely become suppressed (Carr et al. 2018). Shifts in hippocampal AMPA and NMDA receptor mRNA levels are also altered in other similar 1-2 beam models of GCR irradiation (Howe et al., 2019; Kiffer et al., 2018), with computational modeling additionally suggesting that receptor proteins may be particularly susceptible to radiation-induced damage (Bayarchimeg et al., 2019). However, any changes in receptor expression within individual synapses may be offset by the observed reduction in dendritic spines induced by several single-ion irradiation paradigms (Parihar et al. 2015c, 2016; Allen et al. 2020). Overall hippocampal expression of various proteins involved in normal synaptic signaling, including PSD-95, drebrin 1, synapsin 1, and synaptophysin also become shifted following 1-2 beam GCR irradiation paradigms (Carr et al., 2018; Kiffer et al., 2018; Parihar et al., 2016). Nevertheless, determining the net impact of such hippocampus-wide molecular charges on network-level activity is difficult without knowing the specific cell types that are impacted.

In a more functional measurement performed using paired patch-clamp recordings of hippocampal neurons, we observed that 50 cGy proton irradiation increased the extent of connectivity from excitatory pyramidal neurons onto other neurons, although the strength of excitatory signaling between neurons remained unchanged (Lee et al. 2017). Likewise, in the current study we did not observe any impact of mixed-ion GCR irradiation on the overall degree of excitatory synaptic inputs received by CA1 pyramidal neurons. While sEPSC properties were not altered by mixed-ion GCR irradiation, the increased amplitude of inhibitory signaling received by pyramidal neurons was consistent with our prior paired patch-clamp recordings (Lee et al. 2017). In that study, we observed that 50 cGy proton irradiation preferentially increased GABA release from a portion of perisomatically targeting interneurons onto the pyramidal neurons they innervate. The reduction in sIPSC rise times that we observe following mixed-ion GCR irradiation further supports a preferential increase in perisomatic inhibitory inputs, since somatic inhibition produces faster IPSC rise times than dendritic inhibition (Lee et al., 2010; Miles et al., 1996). Thus, our data indicate that mixed-ion GCR irradiation may produce selective disruptions of neuronal activity within the hippocampus.

Enhanced inhibitory signaling onto pyramidal neurons would appear most likely to suppress activity within hippocampal networks. However, there are also instances where increased hyperpolarization of neurons through inhibition actually promotes greater rebound spiking and more synchronized discharges within neuronal circuits (Cobb et al. 1995; Kim and McCormick 1998; Chen et al. 2001). The decreased oscillatory frequency within sharp wave-ripples after mixed-ion GCR irradiation potentially results from the elevated inhibitory signaling being received by CA1 pyramidal neurons. Increasing α-subunit containing $GABA_A$ receptor activation with low dose diazepam mimics the reduced intra-ripple frequency we observed, while similarly producing no change in ripple occurrence or power (Ponomarenko et al. 2004; Koniaris et al. 2011). Intra-ripple frequency slowing may result from elevated $GABA_A$ receptor activation strengthening action potential after-hyperpolarization of basket and bistratified cells within CA1 (Pawelzik et al. 2003). Thereby, the peak firing rates of interneurons driving the high-frequency components of sharp wave-ripples would be reduced (Buzsáki 2015). However, the number of ripples occurring after mixed-ion GCR irradiation likely remain consistent because the excitatory inputs to CA1 from CA3 neurons that trigger sharp wave-ripple onset stay largely unchanged (Ylinen et al. 1995; Csicsvari et al. 2000). Therefore, both our single cell and network activity data indicate that hippocampal GABAergic signaling is perturbed by mixed-ion GCR irradiation.

With mixed-ion GCR irradiation disrupting cellular- and network-level neuronal activity, we were not surprised to observe that performance in multiple aspects of cognitive behavior was likewise diminished. While GCR-irradiated mice retained some ability to encode new memories, as during initial training on the Morris water maze task, such learning is more dependent upon hippocampal theta rhythms (McNaughton et al., 2006) that we do not find to be perturbed. Indeed, hippocampal place cell mapping, a fundamental unit of spatial encoding, can persist when theta oscillations (Brandon et al., 2014) or sharp wave-ripples are disrupted (Jadhav et al., 2012; Kovács et al., 2016). However, sharp wave-ripples are critically involved in the processes of memory consolidation and recall (Buzsáki, 2015; Joo and Frank, 2018), which are perturbed in our behavioral assays. The same α-subunit containing $GABA_A$ receptor agonists that slow the oscillatory frequency of sharp wave-ripples also decrease memory task performance (Cheng et al. 2006; Martin et al. 2009). Furthermore, non-pharmacological, closed-loop interventions that specifically block hippocampal sharp wave-ripples similarly impair spatial memory consolidation (Girardeau et al. 2009), whereas prolonging sharp wave-ripples improves memory recall (Fernández-Ruiz et al., 2019). While clear links exist between the disruptions we observed in hippocampal functional properties and poor performance in memory behavior, mixed-ion GCR irradiation likely also impacted other brain regions. Recognition and spatial memory functions are both impaired in our animals, with these behaviors collectively depending on proper activity of the hippocampus, striatum, medial prefrontal cortex, perirhinal cortex and insular cortex (Bermudez-Rattoni et al. 1991; Riedel et al. 1999; Setlow and McGaugh 1999; Squire et al. 2004; Warburton and Brown 2015), suggesting that the deficits induced by GCR irradiation likely extend broadly throughout the brain.

Internalizing disorders such as anxiety and depression also arise from abnormal nervous system activity that can span diverse brain regions (Pratt 1992; Pawlak et al. 2012; Oakes et al. 2017). Potential shared interactions exist between the other radiation-induced deficits we observe in neuronal signaling and the increased anxiety-like behavior of mice following mixed-ion GCR irradiation. We previously determined that elevated GABAergic signaling following 50 cGy proton irradiation is associated with diminished CB_1-mediated restriction of tonic GABA release (Lee et al. 2017). Similar disruptions of cannabinoid signaling are anxiogenic in mice (Sink et al. 2010; Dono and Currie 2012), suggesting a potential mechanism for the behavioral deficits we observed. Elevated anxiety may also contribute to the neophobia mice appear to display by preferentially avoiding novel objects in the NOR task (Vogel-Ciernia and Wood 2014) and diminished performance in the Morris water maze probe trial (Chapillon and Debouzie 2000) following 30 cGy mixed-ion GCR irradiation. While forced swim testing did not indicate any alterations in depression-like behavior following mixed-ion irradiation, there are limitations to how well that method corresponds to the human condition of depression (Cryan and Mombereau 2004; Chen et al. 2015). Our ability to detect an increase in depression-like behavior may also have been occluded by the tendency of animals with heightened anxiety to display a longer latency to swimming immobility (Estanislau et al. 2011; Bogdanova et al. 2013). Lower dose 5 cGy mixed-ion GCR irradiation generally appeared to be less harmful, inducing few behavioral deficits. While escalating radiation doses most often produce increasingly harmful effects, radiation hormesis can result in hard to predict interactions between cellular damage and compensatory mechanisms (Cortese et al. 2018). Regardless, we see that mixed-ion GCR irradiation is capable of disrupting neuronal processes in a manner that increases behavior associated with an internalizing disorder.

The nervous system disruptions we observe following 5- or 6-beam GCR irradiation are largely consistent with prior single-ion studies (Rabin et al. 2011; Cherry et al. 2012; Haley et al. 2013; Davis et al. 2015; Parihar et al. 2015b, 2016, 2018; Whoolery et al. 2017; Lee et al. 2017; Carr et al. 2018; Jewell et al. 2018; Allen et al. 2020). More recently, other groups have begun to assess the combined neurological impacts of 2-ion (Raber et al. 2015; Kiffer et al. 2018) or 3-ion (Krukowski et al. 2018; Raber et al. 2019) GCR exposures on mice. Proton irradiation combined with ^{16}O or ^{56}Fe induced spatial learning deficits,

reduced CA1 dendritic complexity (Kiffer et al. 2018) and altered cytokine expression (Raber et al. 2015). Mixing proton and ^{16}O irradiation with either ^{4}He (Krukowski et al. 2018) or ^{28}Si (Raber et al. 2019) impaired social interactions, disrupted spatial memory and triggered increased microglia activation. Male animals appear to be more susceptible to negative neurological consequences of multi-ion irradiation (Krukowski et al. 2018). However, our study is the first to examine the nervous system impacts of increasingly realistic GCR exposures containing 4–5 distinct ion species, including with the powerful insights provided by whole-cell and *in vivo* electrophysiological recordings. Our present data also provide the first evidence that multi-ion GCR irradiation produces interrelated neurological disruptions at a neuronal, network and behavioral scale. While our results suggest that single- and multi-ion GCR irradiation produce a similar scope of cognitive deficits, there remains debate concerning how accurately the full GCR spectrum experienced in space must be recapitulated to sufficiently assess the hazards that future astronauts will face (Norbury et al. 2016; Simonsen et al. 2020).

Overall, our study substantially advances understanding of the potential neurological complications from GCR exposures during deep space travel to Mars through increasingly relevant experimental modeling. Technical and practical limitations often necessitate that total dose delivery transpires over the course of minutes, rather than months, resulting in exaggerated dose-rates compared to actual space exposures. We recently examined the consequences of prolonged neutron irradiation, delivered at a space-relevant dose and dose-rate, on brain function (Acharya et al. 2019). As with our mixed-ion GCR exposure, chronic neutron irradiation altered hippocampal synaptic signaling, interfered with network level activity and produced persistent behavioral disruptions. Although neutron radiation is limited in space, GCR interactions with spacecraft materials generate additional albedo neutrons that represent a sizable component (approximately 10–30%) of the overall effective radiation field (Nelson, 2016; Norbury and Slaba, 2014; Slaba et al., 2011). Our neutron data suggest that the negative neurological consequences of charged particle irradiation may arise even during chronic, low dose-rate exposures. In the future, newly developed technologies and approaches will provide improved experimental modeling of the complex GCR spectra, thus allowing fine-tuned assessment of the space radiation risks posed to neurological function (Simonsen et al. 2020). Continuing to probe the mechanisms through which GCR irradiation disrupts the central nervous system remains critical to accurately assess potential risks and facilitate development of targeted treatment strategies.

4. Methods

4.1. Subjects

Male C57BL/6 J mice (JAX) were utilized in these studies and were 6 months old at the time of irradiation. All experiments were approved by the Institutional Care and Use Committees at the Brookhaven National Laboratory, Stanford University and the University of California, Irvine. Procedures involving animals all conform to National Institute of Health and institutional guidelines. Mice were group housed (2-4 per cage), provided enrichment (shredded paper or nestlets), received *ad libitum* access to food (Stanford: 2018 Teklad; UCI: 2020X Teklad; Envigo) and water, and were maintained on a 12 h light/dark cycle throughout the study.

4.2. Irradiation

Mice were exposed to simulated galactic cosmic radiation (**GCR**) in the NASA Space Radiation Laboratory (**NSRL**) at Brookhaven National Laboratory. Mice received a total radiation dose of either 5 cGy or 30 cGy, containing a GCR-relevant mix of ion species consisting of: protons, helium, oxygen, silicon and in some cases iron. Mixed-ion GCR was delivered in either a 5-beam or 6-beam composition, the specifics of which are detailed in Table 1. The ionic compositions of the mixed beams recapitulate many of the most abundant elements in GCR (Nelson 2016) and were delivered at total dose similar to what an astronaut would experience during a voyage to Mars (Zeitlin et al. 2013). Individual mice were loosely restrained within acrylic enclosures ($3 \times 1.5 \times 1.5$ in) mounted perpendicular to the beam line for whole body irradiation at a dose-rate of 5 cGy/min. Irradiation was overseen by NSRL staff, who also performed all radiation dosimetry and confirmed spatial beam uniformity. The low total GCR doses administered produced no observed changes in body weight. Further details on the operation of the NSRL facility have previously been described (La Tessa et al. 2016; Simonsen et al. 2020). Age-matched control mice underwent all aspects of the study in parallel to those receiving irradiation, were housed under similar conditions and handled equivalently, aside from not receiving GCR irradiation. All animals experienced approximately 20 min of enclosed restraint. Following transfer from the NSRL, mice arriving at the University of California, Irvine received no special treatment, whereas animals at Stanford University received prophylactic antiparasitic treatment (fenbendazole, moxidectin and permethrin). Post-irradiation testing was conducted over the course of several months (Fig. S1). With the exception of behavioral testing where multiple assays were conducted in the same mouse, each animal was only used for a single experiment.

4.3. Slice electrophysiology

At 4 months following either 5-beam or 6-beam GCR irradiation, mice were deeply anesthetized with isoflurane and rapidly decapitated. Brains were immediately immersed in ice-cold cutting solution containing (in mM): 85 NaCl, 75 sucrose, 25 glucose, 24 $NaHCO_3$, 4 $MgCl_2$, 2.5 KCl, 1.25 NaH_2PO_4, 0.5 $CaCl_2$. Coronal slices (300 μm) containing the hippocampus were prepared using a vibratome (VTS1200, Leica Biosystems). Brain slices were then incubated in 35 °C cutting solution for 1 h. Prior to recording, brain slices were transferred to aCSF consisting of (in mM): 126 NaCl, 26 $NaHCO_3$, 10 glucose, 2.5 KCl, 2 $MgCl_2$, 2 $CaCl_2$, 1.25 NaH_2PO_4. All solutions were equilibrated with 95% O_2/5% CO_2.

Intracellular recordings were performed in a submerged chamber perfused with oxygenated aCSF at 2.5 ml/min and maintained at 33 °C by a chamber heater (BadController V, Luigs and Neumann). Hippocampal neurons were visualized using DIC illumination on an Olympus BX61WI microscope (Olympus Microscopy) with a CCD camera (C7500, Hamamatsu). Recording pipettes were pulled from thin-walled borosilicate capillary glass (King Precision Glass) using a P97 puller (Sutter Instruments) and were filled with (in mM): 126 K-gluconate, 10 HEPES, 4 KCl, 4 ATP—Mg, 0.3 GTP-Na, 10 phosphocreatine (pH-adjusted to 7.3 with KOH, osmolarity 290 mOsm). Pipettes had a 3–5 MΩ tip resistance.

Whole cell recordings were performed on CA1 superficial layer pyramidal neurons in the dorsal hippocampus (A/P: −1.5–2.4 mm). Firing properties were assessed during current injection steps (−200 to 750 pA, 1 s). Recordings were excluded for neurons with a resting membrane potential above −55 mV or where the series resistance increased by >20% of baseline. Pipette capacitance was neutralized for all recordings. Input resistance was calculated from the change in steady-state membrane potential resulting from hyperpolarizing current injections, while sag was measured as the difference between the steady-state and peak negative potential during a − 100 pA hyperpolarizing current injection. Action potential threshold was the voltage where the dV/dt prior to a detected event first exceeded 3 times the standard deviation. Width was the time an action potential, resampled at 100 kHz, exceeded the half-height between threshold and peak voltages, and cells with a width < 0.75 ms were excluded as potential fast-spiking interneurons. Action potential properties were only measured in the first spike evoked by a depolarizing current for each neuron. sEPSC activity was measured as inward currents while neurons were held at −65 mV, whereas sIPSCs

were outward currents observed in neurons held at 0 mV. Charge transfer was calculated by integrating the area of postsynaptic currents and rise time was the time required to increase from 10% to 90% of peak amplitude. Events with a rise time $>$ 7.5 ms, a peak amplitude of $<$3 pA or a charge transfer of $<$25 pC were excluded. 6-beam GCR intrinsic property were recorded in brain slices obtained from 6 irradiated male mice, with excitatory *versus* inhibitory synaptic signaling each being recorded from 3 of those mice and with equal numbers of control mice being utilized. 5-beam recordings were performed from 4 GCR-irradiated and 2 control animals.

Data were acquired in pClamp software (Molecular Devices) using a Multiclamp 700B amplifier (Molecular Devices), low-pass filtered at 2 kHz, and digitized at 10 kHz (Digidata 1440A, Molecular Devices). Data analysis was performed using Clampfit (Molecular Devices) and custom written Python scripts.

4.4. In vivo electrophysiology

2 months after exposure to 5-beam GCR irradiation, hippocampal oscillations were measured using previously described *in vivo* LFP recording approaches (Varga et al. 2012, 2014). Briefly, one week prior to LFP recording, mice were implanted with head bars while under deep isoflurane anesthesia. Following recovery, mice were acclimated to experimenter handling. On the day of recording, mice were deeply anesthetized with isoflurane and bilateral craniotomies were stereotaxically performed ($-$2.0 mm AP, $\pm$2 mm ML) to allow for access to the dorsal hippocampus. Mice were then head-fixed on an 8-in spherical treadmill and allowed to recover from anesthesia for 30 min, providing time to become fully alert. Two long-tapered borosilicate glass electrodes filled with 0.5 M NaCl were then bilaterally lowered into the CA1 stratum pyramidale, where the position of each was adjusted to obtain maximal amplitude hippocampal sharp wave-ripples. Data were acquired using a Neurodata IR283 amplifier (Cygnus Technology) and digitized at 20 kHz using a NIDAQ data acquisition card (National Instruments), paired with a custom written MATLAB data acquisition scripts. Recordings lasted approximately 30 min to capture at least 10 min of LFP activity while the mouse was resting (composed of individual episodes each lasting $>$200 s) and 1 min while the mouse was running (episodes each $>$20 s). LFP recordings were performed in a static visual field, open to the surrounding experimental setup. Between trials, any solid debris was vacuumed from the spherical treadmill, which was then wiped down with ethanol and allowed to fully dry before the next experiment began.

LFP data was analyzed using custom written MATLAB scripts (Varga et al. 2012). The power of the LFP signal in the theta (4–10 Hz), low gamma (20–55 Hz) gamma (20–95 Hz) and high gamma (85–135 Hz) bands was measured during periods of running. Sharp wave-ripples were defined as high-frequency oscillatory periods while the animal was resting. To detect ripples, the LFP signal was filtered between 90 and 200 Hz and periods where the absolute value of the filtered trace exceeded 5 standard deviations of the overall variability of the trace were identified. Ripples were considered to extend to contiguous periods of activity that reached a threshold of 2 standard deviations above noise. The intra-ripple frequency was the frequency of the oscillations composing ripples and was calculated independently for each ripple event.

4.5. Immunohistochemistry

At 3 months after irradiation with 5-beam GCR, mice were deeply anesthetized with ketamine (100 mg/kg) and xylazine (10 mg/kg), prior to being transcardially perfused with PBS, followed by 4% PFA in PBS. Brains were post-fixed overnight in 4% PFA and then 50 μm thick coronal sections containing CA1 stratum radiatum were obtained using a vibratome (VTS1000S, Leica Biosystems).

Free-floating sections were washed in PB prior to blocking in TBS with 5% normal donkey serum and 0.3% Triton X-100 for 45 min at room temperature. Sections were then incubated for 2 days at 4 °C in combined primary antibodies for VGluT1 and Bassoon in TBS (guinea pig anti-VGluT1, 1:5000, Synaptic Systems, 135–304; mouse anti-Bassoon, 1:3000, Abcam, ab82958). Following primary antibody incubation, sections were washed in TBS, incubated in secondary antibodies (donkey anti-guinea pig Alexa Fluor 594, 1:800, Jackson Immunoresearch, 706–585-148; donkey anti-mouse Alexa Fluor 488, 1:800, Jackson Immunoresearch, 715–545-150) for 4 h at room temperature and then washed again in TBS. Immunostained sections were postfixed in 4% PFA for 10 min prior to washing in PB and mounting on coverslips with Vectashield (Vector Laboratories).

Images were acquired from 3 to 4 fields of 41 μm^2 (512 $\times$ 512 pixels) within CA1 stratum radiatum on 4 tissue sections per animal using a Nikon A1R microscope with a 60$\times$ Plan Apo VC oil immersion objective. Blinded investigators acquired image z-stacks that underwent unbiased deconvolution using Huygens software (Scientific Volume Imaging) and then thresholding in ImageJ. Thresholded objects were further restricted to areas of 50–3000 voxels for VGluT1 and 4–100 voxels for Bassoon, to approximate the sizes of synaptic terminals and active zones, respectively. Colocalization was considered to occur when there was at least 4 voxels of overlap between the two channels.

4.6. Behavioral testing

Behavioral testing of 5-beam GCR irradiated mice and control animals began 6 weeks following irradiation and lasted for 4 weeks. Tests were performed and scored by investigators blinded to the treatment groups of the animals.

4.6.1. Episodic and spatial memory testing

Novel object recognition (**NOR**) spontaneous exploration task performance depends upon normal hippocampal, medial prefrontal cortex and perirhinal cortex function (Barker et al. 2007; Barker and Warburton 2011). The NOR task assesses episodic recognition memory by observing the preference of mice to investigate novel environmental changes and was conducted as described previously (Parihar et al. 2015a). Briefly, NOR was tested in a dimly lit (48 lx) test arena (30 $\times$ 30 $\times$ 30 cm) filmed from above. The arena was thoroughly cleaned with 70% ethanol between trials. Prior to the NOR task, mice were initially habituated to the empty arena across three days (10 min/day). On the following day, two plastic objects were magnetically affixed 16 cm apart in the arena and the mouse was allowed five minutes to interact with the objects. The mouse was returned to the home cage for five minutes while one familiar object was substituted for a novel object (both objects were cleansed with 70% ethanol). The mouse was then returned to the arena for five minutes of further exploration. The objects, varying in area (30–50 cm^2), height (6–9 cm), geometry (e.g. curved or angular) and color (e.g. blue, pink or yellow), were randomized between subjects to minimize the impact of objects with inherently elevated preference. NOR task video was scored for time interacting (nose within 2 cm) with the familiar *versus* novel object. The discrimination index was than calculated for each mouse from these values:

$$[(\text{novel/total exploration time})–(\text{familiar/total exploration time})] \times 100$$

4.6.2. Anxiety- and depression-like behavior testing

At 8 weeks after irradiation, mice were evaluated for anxiety-like behavior with the elevated plus maze (**EPM**) test and depression-like behavior with the forced swim test (**FST**), using established methods (Pellow et al. 1985; Petit-Demouliere et al. 2005; Parihar et al. 2018). The elevated plus maze consisted of two open arms (10 $\times$ 50 cm) connected through a central space to two enclosed arms (10 $\times$ 50 $\times$ 42 cm). Heightened anxiety reduces interest in exploring the more exposed open arms. Mice were initially placed in the center of the EPM, facing towards a closed arm, and were allowed to freely explore for 5 min while their

movement was recorded. A mouse was considered to enter a new arm when all four paws crossed into that space. For the FST task, we evaluated depression-like behavior by measuring the responses of mice to being placed in a glass beaker of water (15 cm diameter × 20 cm, 24 °C) for five minutes. We quantified the time mice spent floating (despair-like behavior) *versus* swimming or climbing.

4.6.3. Morris water maze

A Morris Water Maze (**MWM**) test was used 9 weeks after GCR irradiation to measure impacts on spatial memory. The MWM assay was performed in a circular pool (121.9 cm diameter, 72 cm high) filled with water (20–22 °C) to a depth of 52 cm to prevent escape, with wall-mounted visual cues placed nearby surrounding the pool. A platform (11.43 cm diameter) located 2 cm below the water surface was hidden by making the water opaque using nontoxic white paint. During the 7 training sessions mice participated in 4 trials per day. Each trial began with a mouse being placed in a different quadrant of the tank in a random sequence and then allowed to swim for 60 s or until it found the submerged platform. Training sessions were conducted on consecutive days, except for an additional 2 day pause following session 4, after which the platform was relocated to a different quadrant of the tank. Mice were allowed to remain on the platform for 10 s in order to reinforce the platform quadrant location before being returned to their home cage. Mice unable to locate the platform within 60 s were then assisted to the platform, where they were allowed to remain for 10 s and were assigned a maximum time of 60 s. A probe trial was conducted the day after the 7th training session, where the platform was removed to test memory retrieval. Mice were allowed to swim for 60 s and the times spent searching for the missing platform in each quadrant were analyzed. Performance was tracked by Ethovision XT 8.5 software.

4.7. Statistical analysis

To account for the nested data produced by immunohistochemistry and whole cell electrophysiology experiments, differences between treatment groups were evaluated by a mixed linear model regression analysis (Aarts et al. 2014). For all other assays, differences were determined using *t*-tests or ANOVA measures (with Tukey's HSD post-hoc testing), as noted. Calculation of estimation statistics-based confidence intervals was performed with the DABEST package in Python (Ho et al. 2019). Gardner-Altman and Cumming estimation plots include a 5000 resampling, bias-corrected and accelerated bootstrap analysis to determine the nonparametric confidence interval of differences between groups. We quantified effect sizes with an unbiased *Cohen's d* test. Estimation statistics were not calculated for behavioral assays spanning across multiple time points or for *in vivo* electrophysiology experiments with limited sample sizes, where data are plotted as mean ± SEM. While estimation statistics measures do not assume normality, normality was nevertheless inspected for all measures by generating Q-Q plots. All statistical analysis was performed in Python and *P*-values of ≤ 0.05 were considered to be statistically significant.

Supplementary data to this article can be found online at https://doi.org/10.1016/j.nbd.2021.105252.

Declaration of Competing Interest

The authors declare no competing financial interests.

Acknowledgements

This work was supported by NASA Specialized Center of Research grant NNX15AI22G (CLL, IS) and by the National Research, Development and Innovation Office of Hungary Frontier Program grant 129961 (MZ, IK). Thank you to all members of the NASA Space Radiation Laboratory for their invaluable assistance in the irradiation of animals.

References

Aarts, E., Verhage, M., Veenvliet, J.V., Dolan, C.V., van der Sluis, S., 2014. A solution to dependency: using multilevel analysis to accommodate nested data. Nat. Neurosci. 17, 491–496.
Acharya, M.M., Baulch, J.E., Klein, P.M., Baddour, A.A.D., Apodaca, L.A., Kramár, E.A., Alikhani, L., Garcia, C., Angulo, M.C., Batra, R.S., Fallgren, C.M., Borak, T.B., Stark, C.E.L., Wood, M.A., Britten, R.A., Soltesz, I., Limoli, C.L., 2019. New concerns for neurocognitive function during deep space exposures to chronic, low dose-rate, neutron radiation. eNeuro 6, 1–15.
Al-Jahdari, W.S., Suzuki, Y., Yoshida, Y., Hamada, N., Shirai, K., Noda, S.E., Funayama, T., Sakashita, T., Kobayashi, Y., Saito, S., Goto, F., Nakano, T., 2009. The radiobiological effectiveness of carbon-ion beams on growing neurons. Int. J. Radiat. Biol. 85, 700–709.
Allen, B.D., Syage, A.R., Maroso, M., Baddour, A.A.D., Luong, V., Minasyan, H., Giedzinski, E., West, B.L., Soltesz, I., Limoli, C.L., Baulch, J.E., Acharya, M.M., 2020. Mitigation of helium irradiation-induced brain injury by microglia depletion. J. Neuroinflammation 17, 159.
Asaithamby, A., Chen, D.J., 2011. Mechanism of cluster DNA damage repair in response to high-atomic number and energy particles radiation. Mutat. Res. 711, 87–99.
Autsavapromporn, N., Suzuki, M., Funayama, T., Usami, N., Plante, I., Yokota, Y., Mutou, Y., Ikeda, H., Kobayashi, K., Kobayashi, Y., Uchihori, Y., Hei, T.K., Azzam, E. I., Murakami, T., 2013. Gap junction communication and the propagation of bystander effects induced by microbeam irradiation in human fibroblast cultures: the impact of radiation quality. Radiat. Res. 180, 367–375.
Barker, G.R.I., Warburton, E.C., 2011. When is the hippocampus involved in recognition memory? J. Neurosci. 31, 10721–10731.
Barker, G.R.I., Bird, F., Alexander, V., Warburton, E.C., 2007. Recognition memory for objects, place, and temporal order: a disconnection analysis of the role of the medial prefrontal cortex and perirhinal cortex. J. Neurosci. 27, 2948–2957.
Bayarchimeg, L., Batmunkh, M., Bugay, A.N., Lkhagva, O., 2019. Evaluation of radiation-induced damage in membrane ion channels and synaptic receptors. Phys. Part. Nucl. Lett. 16, 54–62.
Bermudez-Rattoni, F., Introini-Collison, I.B., McGaugh, J.L., 1991. Reversible inactivation of the insular cortex by tetrodotoxin produces retrograde and anterograde amnesia for inhibitory avoidance and spatial learning. Proc. Natl. Acad. Sci. 88, 5379–5382.
Bogdanova, O.V., Kanekar, S., D'Anci, K.E., Renshaw, P.F., 2013. Factors influencing behavior in the forced swim test. Physiol. Behav. 118, 227–239.
Brandon, M.P., Koenig, J., Leutgeb, S., 2014. New and distinct hippocampal place codes are generated in a new environment during septal inactivation. Neuron 82, 789–796.
Brankačk, J., Stewart, M., Fox, S.E., 1993. Current source density analysis of the hippocampal theta rhythm: associated sustained potentials and candidate synaptic generators. Brain Res. 615, 310–327.
Britten, R.A., Davis, L.K., Johnson, A.M., Keeney, S., Siegel, A., Sanford, L.D., Singletary, S.J., Lonart, G., 2012. Low (20 cGy) doses of 1 GeV/u (56)Fe–particle radiation lead to a persistent reduction in the spatial learning ability of rats. Radiat. Res. 177, 146–151.
Buzsáki, G., 2002. Theta oscillations in the Hippocampus. Neuron 33, 1–20.
Buzsáki, G., 2015. Hippocampal sharp wave-ripple: a cognitive biomarker for episodic memory and planning. Hippocampus 25, 1073–1188.
Buzsáki, G., Leung, L.-W.S., Vanderwolf, C.H., 1983. Cellular bases of hippocampal EEG in the behaving rat. Brain Res. Rev. 6, 139–171.
Carr, H., Alexander, T.C., Groves, T., Kiffer, F., Wang, J., Price, E., Boerma, M., Allen, A. R., 2018. Early effects of16O radiation on neuronal morphology and cognition in a murine model. Life Sci. Sp. Res. 17, 63–73.
Chapillon, P., Debouzie, A., 2000. BALB/c mice are not so bad in the Morris water maze. Behav. Brain Res. 117, 115–118.
Chen, K., Aradi, I., Thon, N., Eghbal-Ahmadi, M., Baram, T.Z., Soltesz, I., 2001. Persistently modified h-channels after complex febrile seizures convert the seizure-induced enhancement of inhibition to hyperexcitability. Nat. Med. 7, 331–337.
Chen, L., Faas, G.C., Ferando, I., Mody, I., 2015. Novel insights into the behavioral analysis of mice subjected to the forced-swim test. Transl. Psychiatry 5, 1–9.
Cheng, V.Y., Martin, L.J., Elliott, E.M., Kim, J.H., Mount, H.T.J., Taverna, F.A., Roder, J. C., Macdonald, J.F., Bhambri, A., Collinson, N., Wafford, K.A., Orser, B.A., 2006. Alpha5GABAA receptors mediate the amnestic but not sedative-hypnotic effects of the general anesthetic etomidate. J. Neurosci. 26, 3713–3720.
Cherry, J.D., Liu, B., Frost, J.L., Lemere, C.A., Williams, J.P., Olschowka, J.A., O'Banion, M.K., 2012. Galactic cosmic radiation leads to cognitive impairment and increased Aβ plaque accumulation in a mouse model of Alzheimer's disease. PLoS One 7.
Cobb, S.R., Buhl, E.H., Halasy, K., Paulsen, O., Somogyi, P., 1995. Synchronization of neuronal activity in hippocampus by individual GABAergic interneurons. Nature 378, 75–78.
Cortese, F., et al., 2018. Vive la radiorésistance!: converging research in radiobiology and biogerontology to enhance human radioresistance for deep space exploration and colonization. Oncotarget 9, 14692–14722.
Cryan, J.F., Mombereau, C., 2004. In search of a depressed mouse: utility of models for studying depression-related behavior in genetically modified mice. Mol. Psychiatry 9, 326–357.
Csicsvari, J., Hirase, H., Mamiya, A., Buzsáki, G., 2000. Ensemble patterns of hippocampal CA3-CA1 neurons during sharp wave-associated population events. Neuron 28, 585–594.
Cucinotta, F.A., Durante, M., 2006. Cancer risk from exposure to galactic cosmic rays: implications for space exploration by human beings. Lancet Oncol. 7, 431–435.

Cucinotta, F.A., Schimmerling, W., Wilson, J.W., Peterson, L.E., Badhwar, G.D., Saganti, P.B., Dicello, J.F., 2001. Space radiation cancer risks and uncertainties for mArs missions. Radiat. Res. 156, 682–688.
Cucinotta, F.A., Alp, M., Sulzman, F.M., Wang, M., 2014. Space radiation risks to the central nervous system. Life Sci. Sp. Res. 2, 54–69.
Davis, C.M., DeCicco-Skinner, K.L., Hienz, R.D., 2015. Deficits in sustained attention and changes in dopaminergic protein levels following exposure to proton radiation are related to basal dopaminergic function. PLoS One 10, 1–17.
D'Hooge, R., De Deyn, P.P., 2001. Applications of the Morris water maze in the study of learning and memory. Brain Res. Brain Res. Rev. 36, 60–90.
Ding, L., Shingyoji, M., Chen, F., Chatterjee, A., Kasai, K.-E., Chen, D.J., 2005. Gene expression changes in normal human skin fibroblasts induced by HZE-particle radiation. Radiat. Res. 164, 523–526.
Dobynde, M.I., Shprits, Y.Y., 2020. Radiation environment created with GCRs inside a spacecraft. Life Sci. Sp. Res. 24, 116–121.
Dono, L.M., Currie, P.J., 2012. The cannabinoid receptor CB 1 inverse agonist AM251 potentiates the anxiogenic activity of urocortin i in the basolateral amygdala. Neuropharmacology 62, 192–199.
Durante, M., Orecchia, R., Loeffler, J.S., 2017. Charged-particle therapy in cancer: clinical uses and future perspectives. Nat. Rev. Clin. Oncol. 14, 483–495.
Estanislau, C., Ramos, A.C., Ferraresi, P.D., Costa, N.F., de Carvalho, H.M.C.P., Batistela, S., 2011. Individual differences in the elevated plus-maze and the forced swim test. Behav. Process. 86, 46–51.
Fernández-Ruiz, A., Olivia, A., de Oliveira, E.F., Rocha-Almeida, F., Tingley, D., Buzsáki, G., 2019. Long-duration hippocampal sharp wave ripples improve memory. Science 364, 1082–1086.
Finlay, J.M., Dunham, G.A., Isherwood, A.M., Newton, C.J., Nguyen, T.V., Reppar, P.C., Snitkovski, I., Paschall, S.A., Greene, R.W., 2015. Effects of prefrontal cortex and hippocampal NMDA NR1-subunit deletion on complex cognitive and social behaviors. Brain Res. 1600, 70–83.
George, K., Durante, M., Cucinotta, F.A., 2007. Chromosome aberrations in astronauts. Adv. Sp. Res. 40, 483–490.
Girardeau, G., Benchenane, K., Wiener, S.I., Buzsáki, G., Zugaro, M.B., 2009. Selective suppression of hippocampal ripples impairs spatial memory. Nat. Neurosci. 12, 1222–1223.
Glebov, O.O., Cox, S., Humphreys, L., Burrone, J., 2016. Neuronal activity controls transsynaptic geometry. Sci. Rep. 6, 1–11.
Green, J.D., Arduini, A.A., 1954. Hippocampal electrical activity in arousal. J. Neurophysiol. 17, 533–557.
Haley, G.E., Yeiser, L., Olsen, R.H.J., Davis, M.J., Johnson, L.A., Raber, J., 2013. Early effects of whole-body (56)Fe irradiation on hippocampal function in C57BL/6J mice. Radiat. Res. 179, 590–596.
Ho, J., Tumkaya, T., Aryal, S., Choi, H., Claridge-Chang, A., 2019. Moving beyond P values: data analysis with estimation graphics. Nat. Methods 16, 565–566.
Howe, A., Kiffer, F., Alexander, T.C., Sridharan, V., Wang, J., Ntagwabira, F., Rodriguez, A., Boerma, M., Allen, A.R., 2019. Long-term changes in cognition and physiology after low-dose ^{16}O irradiation. Int. J. Mol. Sci. 20, 1–17.
Huang, E.G., Wang, R.Y., Xie, L., Chang, P., Yao, G., Zhang, B., Ham, D.W., Lin, Y., Blakely, E.A., Sachs, R.K., 2020. Simulating galactic cosmic ray effects: synergy modeling of murine tumor prevalence after exposure to two one-ion beams in rapid sequence. Life Sci. Sp. Res. 25, 107–118.
Jadhav, S.P., Kemere, C., German, P.W., Frank, L.M., 2012. Awake hippocampal sharp-wave ripples support spatial memory. Science 336, 1454–1458.
Jewell, J.S., Duncan, V.D., Fesshaye, A., Tondin, A., Macadat, E., Britten, R.A., 2018. Exposure to ≤15 cGy of 600 MeV/n 56Fe particles impairs rule acquisition but not long-term memory in the attentional set-shifting assay. Radiat. Res. 190, 565–575.
Joo, H.R., Frank, L.M., 2018. The hippocampal sharp wave–ripple in memory retrieval for immediate use and consolidation. Nat. Rev. Neurosci. 19, 744–757.
Kiffer, F., Alexander, T., Anderson, J., Groves, T., McElroy, T., Wang, J., Sridharan, V., Bauer, M., Boerma, M., Allen, A., 2020. Late effects of ^{1}H + ^{16}O on short-term and object memory, hippocampal dendritic morphology and mutagenesis. Front. Behav. Neurosci. 14, 1–15.
Kiffer, F., Carr, H., Groves, T., Anderson, J.E., Alexander, T., Wang, J., Seawright, J.W., Sridharan, V., Carter, G., Boerma, M., Allen, A.R., 2018. Effects of 1 H + 16 O charged particle irradiation on short-term memory and hippocampal physiology in a murine model. Radiat. Res. 189, 53–63.
Kim, U., McCormick, D.A., 1998. The functional influence of burst and tonic firing mode on synaptic interactions in the thalamus. J. Neurosci. 18, 9500–9516.
Ko, J., 2017. Neuroanatomical substrates of rodent social behavior: the medial prefrontal cortex and its projection patterns. Front. Neural Circ. 11, 1–16.
Koniaris, E., Drimala, P., Sotiriou, E., Papatheodoropoulos, C., 2011. Different effects of zolpidem and diazepam on hippocampal sharp wave-ripple activity in vitro. Neuroscience 175, 224–234.
Korotkova, T., Fuchs, E.C., Ponomarenko, A., von Engelhardt, J., Monyer, H., 2010. NMDA receptor ablation on Parvalbumin-positive interneurons impairs hippocampal synchrony, spatial representations, and working memory. Neuron 68, 557–569.
Kovács, K.A., O'Neill, J.O., Schoenenberger, P., Penttonen, M., Ranguel Guerrero, D.K., Csicsvari, J., 2016. Optogenetically blocking sharp wave ripple events in sleep does not interfere with the formation of stable spatial representation in the CA1 area of the hippocampus. PLoS One 11, 1–19.
Krukowski, K., Grue, K., Frias, E.S., Pietrykowski, J., Jones, T., Nelson, G.A., Rosi, S., 2018. Female mice are protected from space radiation-induced maladaptive responses. Brain Behav. Immun. 74, 106–120.
La Tessa, C., Sivertz, M., Chiang, I.H., Lowenstein, D., Rusek, A., 2016. Overview of the NASA space radiation laboratory. Life Sci. Sp. Res. 11, 18–23.
Lee, S.-H., Földy, C., Soltesz, I., 2010. Distinct endocannabinoid control of GABA release at perisomatic and dendritic synapses in the hippocampus. J. Neurosci. 30, 7993–8000.
Lee, R., Nasonova, E., Ritter, S., 2005. Chromosome aberration yields and apoptosis in human lymphocytes irradiated with Fe-ions of differing LET. Adv. Sp. Res. 35, 268–275.
Lee, S.-H., Dudok, B., Parihar, V.K., Jung, K.M., Zöldi, M., Kang, Y.-J., Maroso, M., Alexander, A.L., Nelson, G.A., Piomelli, D., Katona, I., Limoli, C.L., Soltesz, I., 2017. Neurophysiology of space travel: energetic solar particles cause cell type-specific plasticity of neurotransmission. Brain Struct. Funct. 222, 2345–2357.
Limoli, C.L., Ponnaiya, B., Corcoran, J.J., Giedzinski, E., Morgan, W.F., 2000. Chromosomal instability induced by heavy ion irradiation. Int. J. Radiat. Biol. 76, 1599–1606.
Martin, L.J., Oh, G.H.T., Orser, B.A., 2009. Etomidate targets α5 γ-aminobutyric acid subtype a receptors to regulate synaptic plasticity and memory blockade. Anesthesiology 111, 1025–1035.
McNaughton, N., Ruan, M., Woodnorth, M.-A., 2006. Restoring theta-like rhythmicity in rats restores initial learning in the Morris water maze. Hippocampus 16, 1102–1110.
Miles, R., Tóth, K., Gulyás, A.I., Hájos, N., Freund, T.F., 1996. Differences between somatic and dendritic inhibition in the hippocampus. Neuron 16, 815–823.
Miller, R.C., Martin, S.G., Hanson, W.R., Marino, S.A., Hall, E.J., 1998. Effect of track structure and radioprotectors on the induction of oncogenic transformation in murine fibroblasts by heavy ions. Adv. Sp. Res. 22, 1719–1723.
Miyawaki, D., Murakami, M., Demizu, Y., Sasaki, R., Niwa, Y., Terashima, K., Nishimura, H., Hishikawa, Y., Sugimura, K., 2009. Brain injury after proton therapy or carbon ion therapy for head-and-neck cancer and skull base tumors. Int. J. Radiat. Oncol. Biol. Phys. 75, 378–384.
Nelson, G.A., 2016. Space radiation and human exposures, a primer. Radiat. Res. 185, 349–358.
Norbury, J.W., Slaba, T.C., 2014. Space radiation accelerator experiments - the role of neutrons and light ions. Life Sci. Sp. Res. 3, 90–94.
Norbury, J.W., et al., 2016. Galactic cosmic ray simulation at the NASA space radiation laboratory. Life Sci. Sp. Res. 8, 38–51.
Oakes, P., Loukas, M., Oskouian, R.J., Tubbs, R.S., 2017. The neuroanatomy of depression: a review. Clin. Anat. 30, 44–49.
Parihar, V.K., Allen, B.D., Tran, K.K., Chmielewski, N.N., Craver, B.M., Martirosian, V., Morganti, J.M., Rosi, S., Vlkolinský, R., Acharya, M.M., Nelson, G.A., Allen, A.R., Limoli, C.L., 2015a. Targeted overexpression of mitochondrial catalase prevents radiation-induced cognitive dysfunction. Antioxid. Redox Signal. 22, 78–91.
Parihar, V.K., Allen, B.D., Tran, K.K., Macaraeg, T.G., Chu, E.M., Kwok, S.F., Chmielewski, N.N., Craver, B.M., Baulch, J.E., Acharya, M.M., Cucinotta, F.A., Limoli, C.L., 2015b. What happens to your brain on the way to Mars. Sci. Adv. 1, e1400256.
Parihar, V.K., Pasha, J., Tran, K.K., Craver, B.M., Acharya, M.M., Limoli, C.L., 2015c. Persistent changes in neuronal structure and synaptic plasticity caused by proton irradiation. Brain Struct. Funct. 220, 1161–1171.
Parihar, V.K., Allen, B.D., Caressi, C., Kwok, S., Chu, E., Tran, K.K., Chmielewski, N.N., Giedzinski, E., Acharya, M.M., Britten, R.A., Baulch, J.E., Limoli, C.L., 2016. Cosmic radiation exposure and persistent cognitive dysfunction. Sci. Rep. 6, 1–14.
Parihar, V.K., Maroso, M., Syage, A., Allen, B.D., Angulo, M.C., Soltesz, I., Limoli, C.L., 2018. Persistent nature of alterations in cognition and neuronal circuit excitability after exposure to simulated cosmic radiation in mice. Exp. Neurol. 305, 44–55.
Pawelzik, H., Hughes, D.I., Thomson, A.M., 2003. Modulation of inhibitory autapses and synapses on rat CA1 interneurones by GABAA receptor ligands. J. Physiol. 546, 701–716.
Pawlak, C.R., Karrenbauer, B.D., Schneider, P., Ho, Y.J., 2012. The elevated plus-maze test: differential psychopharmacology of anxiety-related behavior. Emot. Rev. 4, 98–115.
Pellow, S., Chopin, P., File, S.E., Briley, M., 1985. Validation of open: closed arm entries in an elevated plus-maze as a measure of anxiety in the rat. J. Neurosci. Methods 14, 149–167.
Petit-Demouliere, B., Chenu, F., Bourin, M., 2005. Forced swimming test in mice: a review of antidepressant activity. Psychopharmacology 177, 245–255.
Ponomarenko, A.A., Korotkova, T.M., Sergeeva, O.A., Haas, H.L., 2004. Multiple GABAA receptor subtypes regulate hippocampal ripple oscillations. Eur. J. Neurosci. 20, 2141–2148.
Pratt, J.A., 1992. The neuroanatomical basis of anxiety. Pharmacol. Ther. 55, 149–181.
Raber, J., Allen, A.R., Sharma, S., Allen, B., Rosi, S., Olsen, R.H.J., Davis, M.J., Eiwaz, M., Fike, J.R., Nelson, G.A., 2015. Effects of proton and combined proton and 56Fe radiation on the Hippocampus. Radiat. Res. 185, 20.
Raber, J., Yamazaki, J., Torres, E.R.S., Kirchoff, N., Stagaman, K., Sharpton, T., Turker, M.S., Kronenberg, A., 2019. Combined effects of three high-energy charged particle beams important for space flight on brain, behavioral and cognitive endpoints in B6D2F1 female and male mice. Front. Physiol. 10.
Rabin, B.M., Carrihill-Knoll, K.L., Shukitt-Hale, B., 2011. Operant responding following exposure to HZE particles and its relationship to particle energy and linear energy transfer. Adv. Sp. Res. 48, 370–377.
Riedel, G., Micheau, J., Lam, A.G.M., Roloff, E.V.L., Martin, S.J., Bridge, H., De Hoz, L., Poeschel, B., McCulloch, J., Morris, R.G.M., 1999. Reversible neural inactivation reveals hippocampal participation in several memory processes. Nat. Neurosci. 2, 898–905.
Rola, R., Sarkissian, V., Obenaus, A., Nelson, G.A., Otsuka, S., Limoli, C.L., Fike, J.R., 2005. High-LET radiation induces inflammation and persistent changes in markers of hippocampal neurogenesis. Radiat. Res. 164, 556–560.

Rola, R., Fishman, K., Baure, J., Rosi, S., Lamborn, K.R., Obenaus, A., Nelson, G.A., Fike, J.R., 2008. Hippocampal neurogenesis and Neuroinflammation after cranial irradiation with 56 Fe particles. Radiat. Res. 169, 626–632.
Setlow, B., McGaugh, J.L., 1999. Involvement of the posteroventral caudate-putamen in memory consolidation in the Morris water maze. Neurobiol. Learn. Mem. 71, 240–247.
Shukitt-Hale, B., Lau, F.C., Cheng, V., Luskin, K., Carey, A.N., Carrihill-Knoll, K.L., Rabin, B.M., Joseph, J.A., 2013. Changes in gene expression in the rat Hippocampus following exposure to 56Fe particles and protection by berry diets. Cent. Nerv. Syst. Agents Med. Chem. 13, 36–42.
Simonsen, L.C., Slaba, T.C., Guida, P., Rusek, A., 2020. NASA's first ground-based galactic cosmic ray simulator: enabling a new era in space radiobiology research (Misteli T, ed.). PLoS Biol. 18, e3000669.
Sink, K.S., Segovia, K.N., Sink, J., Randall, P.A., Collins, L.E., Correa, M., Markus, E.J., Vemuri, V.K., Makriyannis, A., Salamone, J.D., 2010. Potential anxiogenic effects of cannabinoid CB1 receptor antagonists/inverse agonists in rats: comparisons between AM4113, AM251, and the benzodiazepine inverse agonist FG-7142. Eur. Neuropsychopharmacol. 20, 112–122.
Slaba, T.C., Blattnig, S.R., Clowdsley, M.S., 2011. Variation in lunar neutron dose estimates. Rad. Res. 176, 827–841.
Slaba, T.C., Blattnig, S.R., Norbury, J.W., Rusek, A., La Tessa, C., 2016. Reference field specification and preliminary beam selection strategy for accelerator-based GCR simulation. Life. Sci. Sp. Res. 8, 52–67.
Sokolova, I.V., Schneider, C.J., Bezaire, M.J., Soltesz, I., Vlkolinsky, R., Nelson, G.A., 2015. Proton radiation alters intrinsic and synaptic properties of CA1 pyramidal neurons of the mouse Hippocampus. Radiat. Res. 183, 208–218.
Soltesz, I., Deschênes, M., 1993. Low- and high-frequency membrane potential oscillations during theta activity in CA1 and CA3 pyramidal neurons of the rat hippocampus under ketamine-xylazine anesthesia. J. Neurophysiol. 70, 97–115.
Squire, L.R., Stark, C.E.L., Clark, R.E., 2004. The medial temporal lobe. Annu. Rev. Neurosci. 27, 279–306.
Vanderwolf, C.H., 1969. Hippocampal electrical activity and voluntary movement in the rat. Electroencephalogr. Clin. Neurophysiol. 26, 407–418.
Varga, C., Golshani, P., Soltesz, I., 2012. Frequency-invariant temporal ordering of interneuronal discharges during hippocampal oscillations in awake mice. Proc. Natl. Acad. Sci. 109, E2726–E2734.
Varga, C., Oijala, M., Lish, J., Szabo, G.G., Bezaire, M.J., Marchionni, I., Golshani, P., Soltesz, I., 2014. Functional fission of parvalbumin interneuron classes during fast network events. Elife 3, 1–23.
Vogel-Ciernia, A., Wood, M.A., 2014. Examining object location and object recognition memory in mice. Curr. Protoc. Neurosci. 2014, 8.31.1–8.31.17.
Warburton, E.C., Brown, M.W., 2015. Neural circuitry for rat recognition memory. Behav. Brain Res. 285, 131–139.
Ward, J.F., 1994. The complexity of DNA damage: relevance to biological consequences. Int. J. Radiat. Biol. 66, 427–432.
Whoolery, C.W., et al., 2017. Whole-body exposure to 28 Si-radiation dose-dependently disrupts dentate gyrus neurogenesis and proliferation in the short term and new neuron survival and contextual fear conditioning in the long term. Radiat. Res. 188, 532–551.
Ylinen, A., Bragin, A., Nádasdy, Z., Jandó, G., Szabó, I., Sik, A., Buzsáki, G., 1995. Sharp wave-associated high-frequency oscillation (200 Hz) in the intact hippocampus: network and intracellular mechanisms. J. Neurosci. 15, 30–46.
Zeitlin, C., Hassler, D.M., Cucinotta, F.A., Ehresmann, B., Wimmer-Schweingruber, R.F., Brinza, D.E., Kang, S., Weigle, G., Böttcher, S., Böhm, E., Burmeister, S., Guo, J., Köhler, J., Martin, C., Posner, A., Rafkin, S., Reitz, G., 2013. Measurements of energetic particle radiation in transit to Mars on the Mars science laboratory. Science 340, 1080–1084.